UNIVERSIDAD DE INVESTIGACIÓN DE TECNOLOGÍA EXPERIMENTAL YACHAY

Escuela de Ciencias Químicas e Ingeniería

TÍTULO:
"Synthesis, Characterization and Cytotoxic Evaluation of Ag(I) NHC Complexes Derived from Theophylline"

Trabajo de integración curricular presentado como requisito para la obtención de título de Químico

Autor:

Alejandro Rodrigo Pico Pérez

Tutor:

Juan Pablo Saucedo Ph.D.

Co-tutor:

David Morales-Morales Ph.D.

Urcuquí, Marzo 2024

AUTORÍA

Yo, **Pico Pérez Alejandro Rodrigo**, con cédula de identidad 180463236-0, declaro que las ideas, juicios, valoraciones, interpretaciones, consultas bibliográficas, definiciones y conceptualizaciones expuestas en el presente trabajo; así cómo, los procedimientos y herramientas utilizadas en la investigación, son de absoluta responsabilidad de el autor del trabajo de integración curricular. Así mismo, me acojo a los reglamentos internos de la Universidad de Investigación de Tecnología Experimental Yachay.

Urcuquí, Marzo 2024

Alejandro Rodrigo Pico Pérez

CI: 180463236-0

AUTORIZACIÓN DE PUBLICACIÓN

Yo, **Pico Pérez Alejandro Rodrigo**, con cédula de identidad 180463236-0, cedo a la Universidad de Investigación de Tecnología Experimental Yachay, los derechos de publicación de la presente obra, sin que deba haber un reconocimiento económico por este concepto. Declaro además que el texto del presente trabajo de titulación no podrá ser cedido a ninguna empresa editorial para su publicación u otros fines, sin contar previamente con la autorización escrita de la Universidad.

Asimismo, autorizo a la Universidad que realice la digitalización y publicación de este trabajo de integración curricular en el repositorio virtual, de conformidad a lo dispuesto en el Art. 144 de la Ley Orgánica de Educación Superior.

Urcuquí, Marzo 2024.

Alejandro Rodrigo Pico Pérez
CI: 180463236-0

Dedication

Dedicated to my parents, sister, and grandmother. They have been there my whole life, teaching me to work hard and show me the importance of being a good person. This work is dedicated to them so that they can know all their efforts to help me grow into who I am now was not in vain. To my mom, I will love you to the moon and back. I have never seen such a hard-working person in my life. She always sacrifices herself so that I can have the best opportunities. My dad always cheered us up no matter the situation, there with a smile being positive most of the time, I have always loved your stories and I will listen to them a million times. My sister, my guide, my friend, and my other half since I can remember always fighting, crying, laughing, and talking with me, I do not know what life could have been without you by my side, you always believed in me even when I could not. And my grandma ("mi Bachita"), the stone of the whole family, the one I have admired my whole life, the woman who fights against everything, there has been always a flame of a hard-working, lovely woman, the same flame I see in my mother and sister, the one whose eyes shine when her family is together. I am sure that there is not enough life to thank God for giving me my mom, my dad, my sister, and my grandma.

Alejandro Rodrigo Pico Pérez

Acknowledgements

x

Resumen

Productos naturales como la teofilina, la cafeína o la teobromina han llamado la atención por formar complejos organometálicos debido a sus aplicaciones farmacéuticas. En este sentido, la estructura de teofilina es un excelente precursor para la preparación de complejos activos de carbenos N-heterocíclicos (NHC) para favorecer los enlaces metal-carbono con casi cualquier metal de transición; han demostrado ser efectivos en la obtención de compuestos organometálicos que muestran actividades en diferentes campos como el catálisis, farmacéutico y ciencia de materiales entre otros.

En este trabajo, se sintetizaron y caracterizaron una serie de cinco complejos Ag(I) teofilina-NHC, con diferentes grados de substitución con Flúor, utilizando técnicas analíticas como FT-IR, HPLC, RMN, espectroscopia de masas y difracción de rayos X de monocristal.

Se realizaron ensayos preliminares in vitro sobre la actividad anticancerígena de la serie de complejos obtenidos en seis líneas celulares de cáncer humano; glía del sistema nervioso central (U251), próstata (PC-3), leucemia (K562), colon (HCT-15), mama (MCF-7), pulmón (SKLU-1) y en comparación con la línea celular de riñón de mono sano (COS-7). Los resultados muestran que los cinco complejos Ag(I) NHC sintetizados presentan alta potencia y especificidad hacia las líneas de cáncer U-251 y K-562.

Palabras clave: carbenos N-heterocíclicos, líneas celulares de cáncer, teofilína y evaluación citotóxica

Abstract

Natural products such as theophylline, caffeine, or theobromine have caught the attention to form organometallic complexes due to their pharmaceutical applications. In this sense, theophylline structure is an excellent scaffold for the preparation of NHC active complexes to favor metal-carbon bonds with almost any transition metal; have shown to be effective in obtaining organometallic compounds that show activities in different fields such as catalysis, pharmaceutical, and material science among others. In this work, a series of five Ag(I) theophylline-NHC complexes including fluorinated were synthesized and characterized using analytical techniques such as FT-IR, HPLC, NMR, mass spectroscopy, and single-crystal X-ray diffraction. Preliminary in vitro assays on the anticancer activity of five complexes obtained were performed in six human cancer cell lines; central nervous system glia (U251), prostate (PC-3), leukemia (K562), colon (HCT-15), breast (MCF-7), lung (SKLU) and compared with health monkey kidney cell line (COS-7). The results show that all five synthesized Ag(I) NHC complexes present high potency and specificity toward U-251 and K-562.

Keywords: Nitrogen-heterocyclic carbene, cancer cell line, theophylline, and cytotoxic evaluation

Contents

List of Figures

List of Tables

Chapter 1

Background

In recent years chemists around the world have been focused on four main research topics, waste treatment, renewable energies, materials science, and health improvement. Considering the impact on society of the last topic, chemists develop new drugs to act over cancer cells.

Cancer has been present in all human history, sometimes overshadowed by infectious illnesses. World data about cancer has increased in recent years, so nowadays we have a better overview of how this problem affects our world. In 2019, cancer was in the top 10 global causes of death reported by the World Health Organization (WHO).[1] Specifically in Ecuador, we observed that there was an incidence of 19,074 cases and a mortality of 9,941 cases in 2020.[2] However, there are relevant differences between countries and regions due to prevention measurements and diagnosis at a later stage.[3] In 2020, the total number of new cases (both sex and all ages) is 19 292 789 cases and the total number of deaths is 9 958 133 deaths (both sex and all ages).[4] For almost half of the cases, platinum compounds are used to treat cancer. Three main platinum-based chemo-therapeutics are used worldwide for solid tumors: cisplatin, carboplatin, and oxaliplatin; which, show good results in the innovation of cancer cells. For bladder, cervical, ovarian, testicular cancer, non-small cell lung cancer, mesothelioma, and head-and-neck squamous cell carcinoma, it is used cisplatin, which is approved by the U.S. Food and Drug Administration (FDA). For colon and pancreatic cancer, it is used oxaliplatin. For ovarian and lung cancer, it is used carboplatin.[5] However, the serious secondary effects of compounds such as carboplatin, oxaliplatin, and cis-platin create the necessity to look for other compounds that can provide less harmful secondary effects and obtain the same or better efficiency.

1.1   N-Heterocyclic Carbene (NHC) Ligands

1.1.1   Carbene definition

A carbene is a neutral divalent specie, containing six electrons and has sp^2 hybridization. Four electrons are in bonds, and two are unpaired (non-bonding electrons). When the unpaired electrons have opposite spins, the carbene is called singlet carbene ($\sigma^2 p_\pi^0$); in the ground state, the electrons are in the same orbital. When the unpaired electrons have parallel spins (in the ground state, they are in separate orbitals), the carbene is a triplet ($\sigma^1 p_\pi^1$).[6]

Figure 1.1 shows that carbon atoms in carbenes, both singlet, and triplet, have a formal charge of zero. It is important to consider that carbenes, for having unpaired electrons, are not carbocations, carbanions, or radicals.
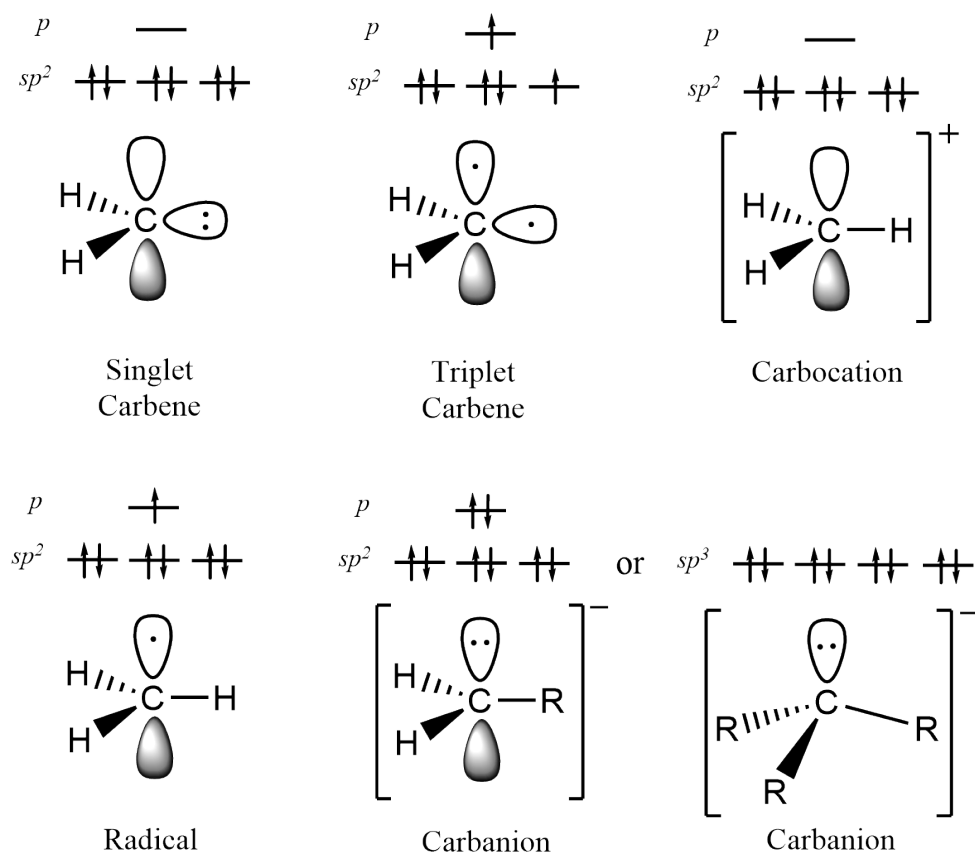
FIGURE 1.1: Species of carbon: carbocation, carbanion, radical and carbene.[6]

1.1.2 Metallic Carbenes

Transition metal carbenes ($L_n = MR_2$) can be broadly described into two types: Fischer-type carbenes and Schrock-type complexes, considering that metal-carbene interactions have a direct relationship with the energetic gap between the carbene (n_σ) and p_π frontier orbitals. Fischer-type carbenes are considered electrophilic at the carbene carbon (C_α). Also, 18 electron complexes have strong $\pi-$acceptors at the metal (figure 1.2-a); then, they are typically low-valent; furthermore, the electronic state of the carbene is a singlet ($\sigma^2 p_\pi^0$), in which the bond is formed by the interaction of the electron pair of the carbene σ orbital and the metal d_z^2 orbital and the reduced π back donation from the metal d_{xy} orbital to the carbene p_π orbital. Fischer-type carbene usually coordinates with metals from groups 8 and 12 in a low oxidation state. They have π-acceptor ligands (L) and π-donor substituents (R) such as $-OMe$.

a) Fischer Type Carbene
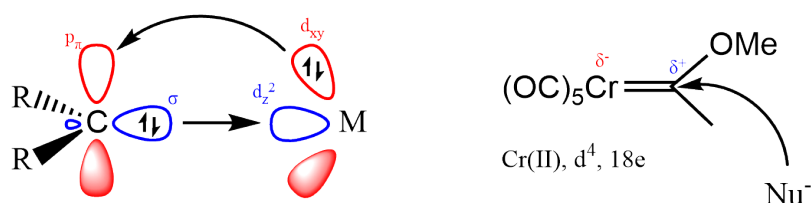
b) Schrock Type Carbene
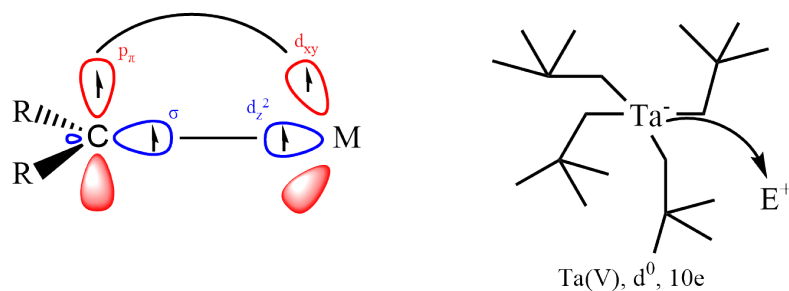
FIGURE 1.2: Typical Fischer type and Schrock type complexes.[7]

Schrock-type carbenes usually behave us carbon nucleophiles (figure 1.2-b); these carbenes have two covalent bonds by the interaction of the triplet carbene ($\sigma^1 p_\pi^1$) and two unpaired electrons from the metal. These carbenes usually coordinate with metals from groups 3 and 7 in a high oxidation state and the substituents (R) are limited to alkyl groups and hydrogen. Also, Schrock carbene contains a strong back-bonding metal.[7–9]

Frontier orbitals control the reactivity of non-heteroatom-stabilized carbene complexes. A critical criterion for the reactivity is the energies of the highest occupied molecular orbital (HOMO) and the lowest occupied molecular orbital (LUMO) of carbene complexes which are determined by the amount of orbital overlap and by the energy difference between carbene $2p$ orbitals and a d orbital of the group $L_n M$. Energy-rich π^* orbital is obtained by complexes with strong π interaction between the metal and the carbene, which are not a good substrate for nucleophilic additions. Furthermore, complexes with high d(metal)-2p(carbon) overlap, electrons will tend to be transferred to a greater extent from the metal to the electron-deficient (more electronegative) C_α. Then, electrophilic attack at C_α atom is facilitated due to partial negative charge and electron density at this atom.

On the other hand, energetically low-lying π^* orbital is obtained by complexes with weak π interaction between the metal and the carbene. Moreover, a positively charged carbene fragment is obtained due to electron transfer from the metal to C_α will be less efficient. Consequently, complexes with large energy gaps and poor orbital overlap between the metal d orbital, and the carbene $2p$ orbital will react with nucleophiles.

To recapitulate, in Fischer-type carbene complexes, the donation of a lone pair of the carbene (n_σ) to metal-vacant orbital results in the metal-carbon $\sigma-$bond; and, the metal-carbon $\pi-$bond is a result from the back-donation from a metal orbital to the carbene vacant p_π orbital (figure 1.3-a). Alternatively, Schrock-type carbene complexes can be described as the interaction between two triplet fragments leading to a covalent metal-carbon double bond (figure 1.3-b).[7,9]

a) Fischer type carbene complex

b) Schrock type carbene complex
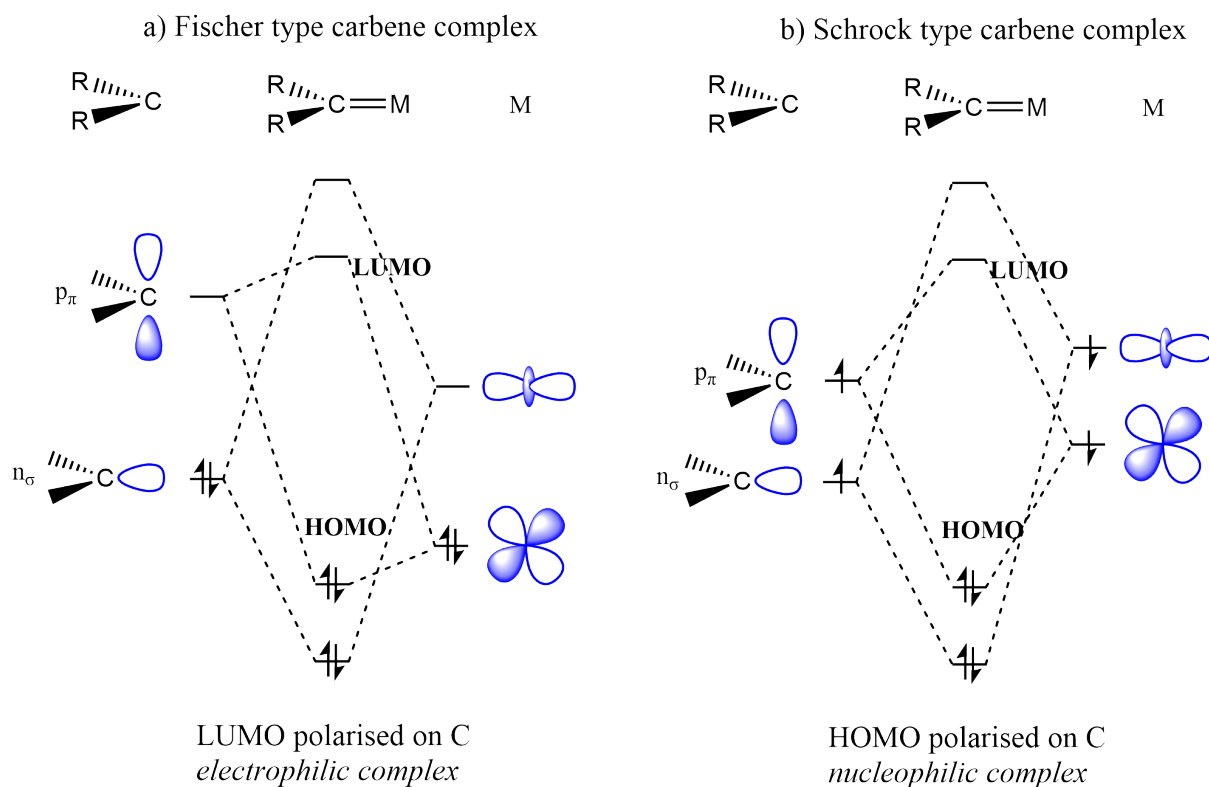
FIGURE 1.3: Molecular orbitals for Fischer type and Schrock type complexes.[9]

1.1.3 Chemical Properties of N-Heterocyclic Carbenes (NHCs)

N-heterocyclic carbenes (NHCs) are neutral, cyclic organic compounds with at least one nitrogen atom within their ring and one divalent carbene atom bearing a lone pair of electrons.[10] The carbene-carbon is considered unstable and reactive, considering that it disobeys the octet rule as it has six valence electrons. NHCs can be classified as classic NHC or mesoionic carbenes. In the case of heteroatom not being attached to the carbene center, the NHC is called 'remote'. Classic NHCs are those obtained from imidazole-2-ylides and 1,2,4-triazolylidenes (figure 1.4, a-c). NHCs are classified as mesoionic carbenes when derived from 1,2,3-triazol-5-ylidenes and imidazol-4-ylidenes (figure 1.4, d-g).[11]
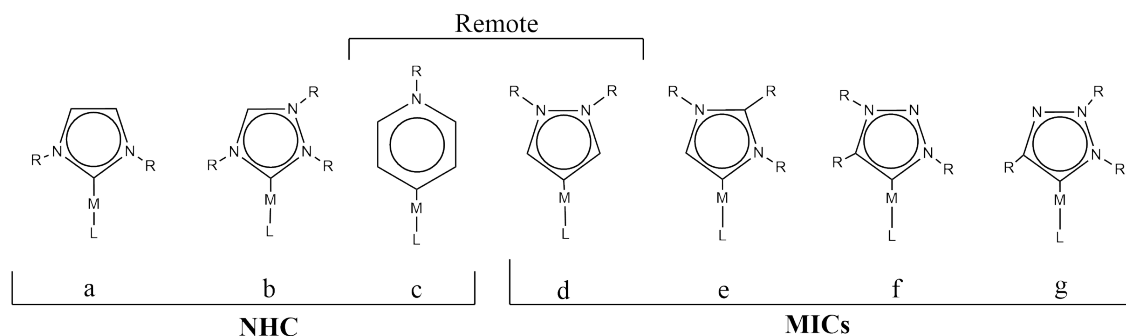
FIGURE 1.4:   General classification of N-heterocyclic carbene-metal complexes).[11]

NHC is usually classified as singlet carbenes because of the presence of two $\pi-$ electron-donating nitrogen atoms next to the carbene carbon, in which the two electrons are located in the σ orbital, while the p_π orbital perpendicular to the carbene plane is formally vacant. The unusual stability of NHCs, which lets them be stored for long periods under an inert atmosphere, is attributed to the "*push-pull effect*" between the nitrogen and the carbene carbon (figure 1.5). The "*pull effect*" is the *negative inductive effect* (*-I* effect) because of the higher electronegativity of the nitrogen atom compared to that of carbon, resulting in the withdrawal of electron density at the carbene center, stabilizing the σ orbital. The "*push effect*" is the *positive mesomeric effect* (*+M* effect), in which the presence of a lone pair at the nitrogen atom allows the delocalization and $\pi-$donation into the formal vacant p_π-vacant orbital of the carbene carbon, increasing its electron density.[7,10,11]
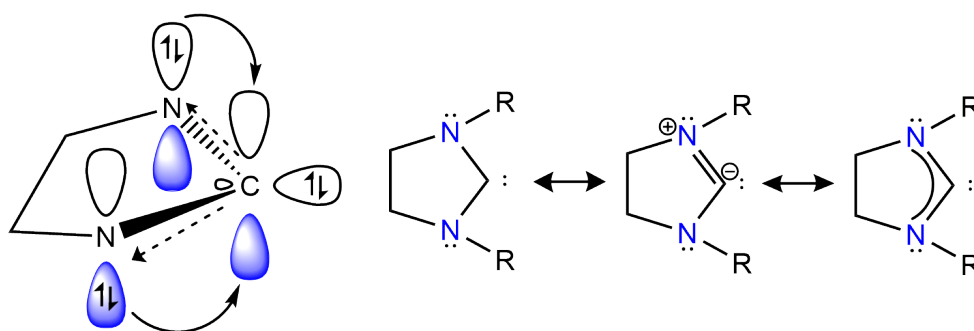
FIGURE 1.5:   Combined *"Push-pull effect"* in imidazolidin-2-ylidene NHC due to *-I* effect (dotted arrow) and *+M* effect (bowed arrow).[12]

1.1.4 Synthetic Aspects of NHC complexes

N-heterocyclic carbenes (NHCs) are organic compounds that mimic the function of phosphines. However, free NHCs us synthetic tools are too reactive. Then, most of them are obtained from azolium salts. NHCs complexes can be prepared by different methods (figure 1.6) such as (a) coordination of free NHCs; (b) cleavage of electron-rich entetramines by transition metals; (c) *in situ* deprotonation of azolium salts in the presence of transition metals; (d) metal carbene transfer routes (Ag, Mo, Cu, etc.); (e) oxidative addition of an azolium salt to a low-valent metal complex; (f) metal-template synthesis using isocyanide complexes as precursors; (g) NHC complexes by small molecule elimination; and (h) NHC complexes by protonation/alkylation of azolyl complexes.[10,11]
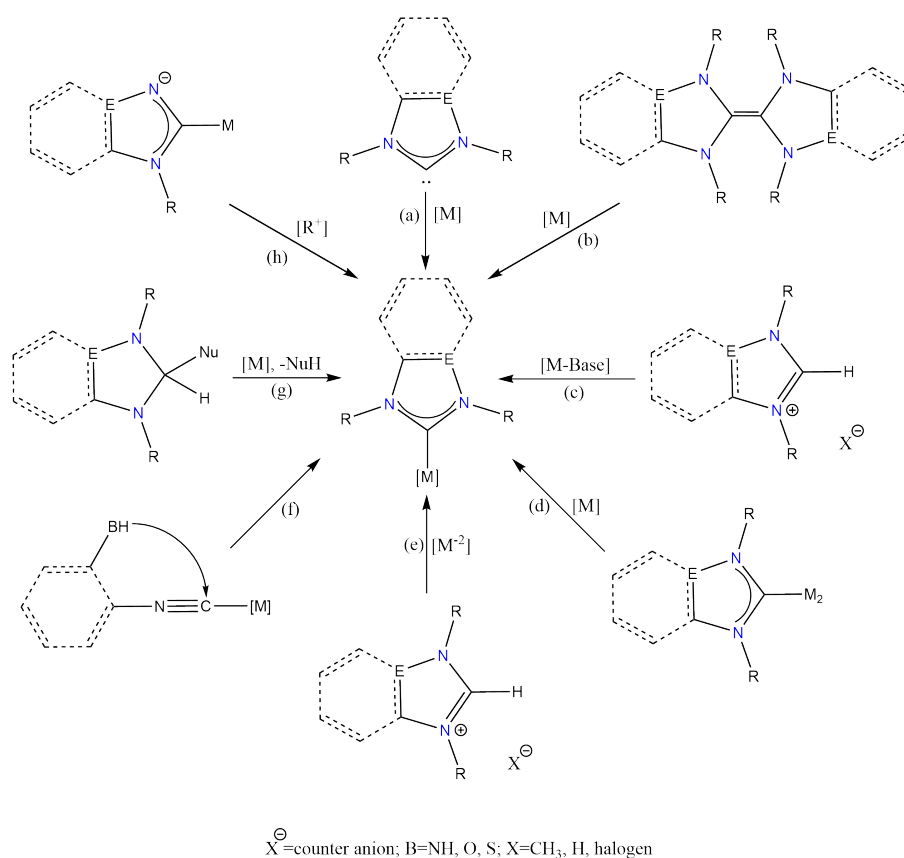
FIGURE 1.6: Major synthetic routes to NHC complexes; (a) coordination of free NHCs; (b) cleavage of electron-rich entetramines by transition metals; (c) *in situ* deprotonation of azolium salts in the presence of transition metals; (d) metal carbene transfer routes (Ag, Mo, Cu, etc.); (e) oxidative addition of an azolium salt to a low-valent metal complex; (f) metal-template synthesis using isocyanide complexes as precursors; (g) NHC complexes by small molecule elimination; and (h) NHC complexes by protonation/alkylation of azolyl complexes.[10]

Considering that to synthesize azolium salts, the best option is the N-alkylation of azoles (figure 1.6, (h)) due to the negative charge in the N, it can be considered for modifications in the nitrogens of the NHC, which is not observed in all the other proposed paths which have fixed ramifications in the N from the NHC. For the preparation of azolium salts, alkyne groups in both nitrogen atoms from the azole ($N1$ and $N3$) are required. The first alkylation requires adding a base such as hydroxides or carbonates of alkaline metals; which will deprotonate the hydrogen from N^3 to form a nucleophilic azolate. Then, a nucleophilic substitution with the alkyl halide ($R_1 - X$). After that, the second N-alkylation occurs with the same alkyl halide ($R_1 - X$) or another alkyl halide ($R_2 - X$). When having two different alkyl halides, it is necessary to have two synthetic steps (figure 1.7).[13]

FIGURE 1.7: Synthesis of azolium salts by N-alkylation.[12]

There are many solvents for N-alkylation, such as polar aprotic solvents (acetonitrile or THF), which are used for the first N-alkylation to solubilize reactants and dissolve the base. Meanwhile, the second N-alkylation usually uses less polar solvents such as DMC or 1,2-DCE; so, the azolium salt completely precipitates. Toluene can be used due to its high boiling point if it needs heat for synthesis.[14]

1.1.5 Applications of Metal-NHC Complexes

NHCs have been considered interesting ligands in organometallic chemistry due to the huge number of topologies that can be obtained, and therefore they can be tuned.[15–19] NHCs have been used as carriers of many transition metals. NHCs complexes have been widely used in medicinal chemistry as potent antibacterial agents, chemo-therapeutics, and antitumor agents; as there is an increasing interest in new drug development to avoid or reduce side effects. Initially, metal-NHC complexes were used for catalytic applications such as Suzuki-Miyaura cross-coupling[20], Mizoroki-Heck cross-coupling[21], etc. Other applications include material science, to be used

as photoactive sites in luminescent materials, for self-assembly into liquid crystalline materials and metallosupramolecular structures.[22,23]

Theophylline, as caffeine or theobromine, is an alkaloid closely related to nucleobases of DNA or RNA, which widely occurs in nature, in the cacao tree.[22] Another valuable feature of theophylline as an NHC precursor is its suitable structure for synthetic applications. As will be shown, one of the nitrogen atoms of this compound can be easily deprotonated via substitution reaction.

Theophylline is a natural NHC compound, it is safe, and easy to get from natural sources. Also, theophylline's multiple properties, such as relation to nucleobases of RNA or DNA, easy edition of the molecule in the N atoms in the cycle by deprotonation, and stability in normal conditions make it attractive for application in the synthesis of metal drugs. Then, theophylline can be used as a modified scaffold structure and it has a wonderful potential to be used as a ligand for anti-tumor drugs. Yuan therefore developed a combination of theophylline and 1,2,3-triazole, to develop a series of safe drugs for the treatment of non-small cell lung cancer (NSCLC). The theophylline acetic acid derivatives (figure 1.8), were tested in two tumor cell lines, A549 (adenocarcinoma human alveolar basal epithelial cells) and MCF-7 (human breast cancer cell line with estrogen, progesterone, and glucocorticoid receptors), as treatment objects. Using CCK8 (Cell Counting Kit - 8) assay was used to evaluate the effect of the series of theophylline acetic acid derivatives on A549 and MCF-7. In table 1.1, both A549 and MCF-7 are not sensitive to theophylline acetic acid ($IC_{50} > 100 \mu M$). A549 was only sensitive to the 4-c compound ($IC_{50} = 6.76 \pm 0.25$) but not sensitive to theophylline acetic acid and other theophylline-1,2,3-triazole derivatives. For MCF-7, 4-a ($IC_{50} = 60.97 \pm 9.74$), 4-b ($IC_{50} = 45.24 \pm 3.23$), 4-c ($IC_{50} = 12.61 \pm 3.48$), 4-d ($IC_{50} = 59.01 \pm 2.68$), and 4-e ($IC_{50} = 80.69 \pm 17.77$) are sensitive. Although the number of compounds sensitive to MCF-7 is more than A549; which has the best sensitivity to the compound 4-c ($IC_{50} = 6.76 \pm 0.25$), MCF-7 gives an intermediate sensitivity to compound 4-c.[24]

4-a, n= 0, R_1= CH_3, R_2= NO_2, R_3= H, R_4= H, R_5= H
4-b, n= 1, R_1= H, R_2= H, R_3= Cl, R_4= H, R_5= H
4-c, n= 0, R_1= CF_3, R_2= H, R_3= H, R_4= CF_3, R_5= H
4-d, n= 0, R_1= Cl, R_2= H, R_3= H, R_4= H, R_5= H
4-e, n= 0, R_1= Br, R_2= H, R_3= H, R_4= H, R_5= H
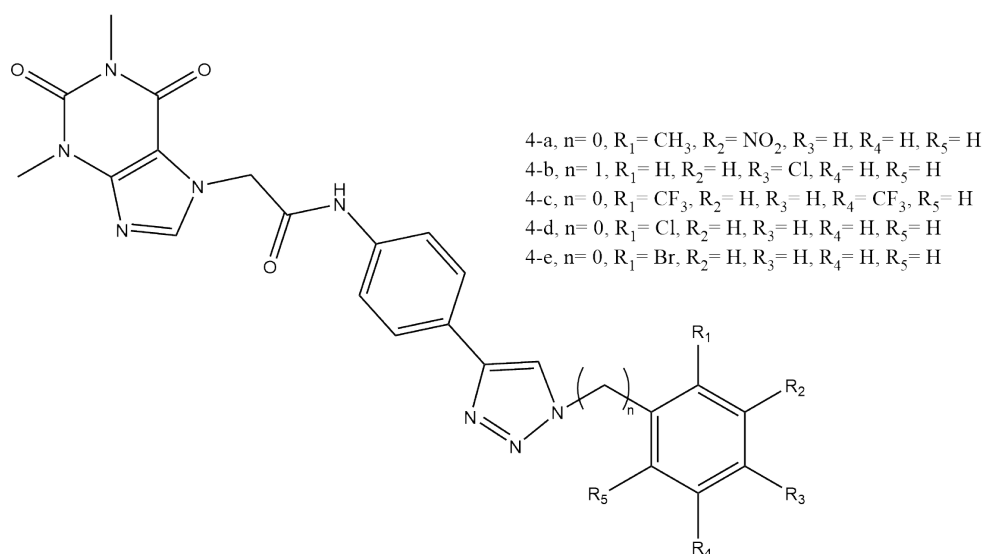
FIGURE 1.8:   Structure of theophylline derivatives by Yuan and coworkers.[24]

Compound	A549	MCF-7
4-a	>100	60.97±9.74
4-b	>100	45.24±3.23
4-c	6.76±0.25	12.61±3.48
4-d	>100	59.01±2.68
4-e	>100	80.69±17.77

TABLE 1.1: $IC_{50}(\mu M)$ values for the antitumor activity of the compounds 4-a,b,c,d,e against two cancer cell lines *in vitro*.[24]

1.1.6   Ag(I) Metallodrugs

Beginning with the isolation of the first stable N-heterocyclic carbene (NHC) by Arduengo in 1991, NHCs have been targeted for research projects in many areas of interest. There have been three main types of NHC structures used as ligands in silver complexes, and all are imidazole-based: imidazolidin-2-ylidene, imidazole-2-ylidene, and benzimidazol-2-ylidene.[25] These ligands can be structurally modified in the side chains of the nitrogen atoms, causing a series of variations in steric and electronic properties of the ligand, which influences the lipophilicity, solubility, and stability of the complexes.

Silver is considered a soft, white, shiny, and lustrous transition metal with the highest electrical conductivity, thermal conductivity, and reflectivity of any metal. Also, Silve anion in pure solvents shows a tetrahedral geometry of coordination, and it

presents a linear geometry under exposure to ligands such as ammonia, this is explained by the silver anion's tendency to sd-hybridization. It is considered a Pearson soft acid due to its big size and low charge. It has a redox potential of 0.7996 for the pair Ag^+/Ag. In some cases such as Ag_2O, Ag compounds can be degraded by exposure to light. Furthermore, NHC-silver complexes can be easily prepared from azolium salts and a suitable silver salt.

When Ag(I)-NHC complexes were studied and their utility discovered, all these compounds gained much interest. Figure 1.9 shows some of the lead antimicrobial compounds developed by the Tacke research group, which show high antibacterial activity (with clearance areas of 10-12 mm). The enhanced antibacterial activity of these compounds was obtained from the increased penetration through the lipid membrane.[25,26]
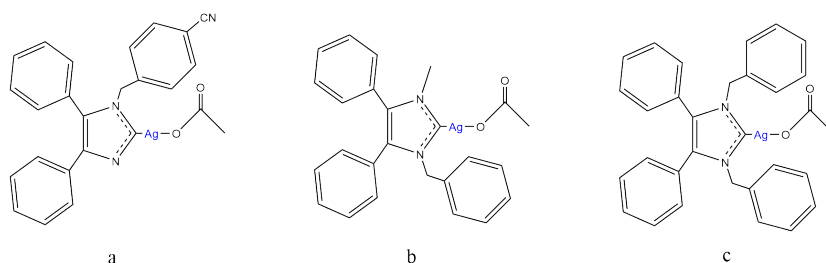
FIGURE 1.9: Structures of Ag(I)-NHC complexes synthesized by Tacke and coworkers.[26]

There is a correlation between tumor development and a state of chronic inflammation, which are strictly connected. A series of anti-inflammatory drugs are to be tested as they appear to suppress the inflammatory process, which can help in cancer treatment. Then, silver carbene compounds can be eligible candidates in the search for cisplatin alternatives and strong antimicrobial agents for the control of infectious diseases.[11,15,25,26]

Metals such as Ag and Au from group 11 have gained much attention for biological and bioinorganic applications because of their low toxicity and biocompatibility; which are desired characteristics for designing anticancer compounds. Here silver has no known biological role, however, it has a promising activity as an antibacterial.

Gust and co-workers describe a series of Ag(I) and Au (I/III) NHC complexes derived from 4,5-diarylimidazole (figure 1.10), and they have evaluated their cytotoxic activity against three cancer cell lines (table 1.2); breast cancer, MCF-7, and MDA-MB-231; colon cancer cells, HT-29. This study shows that Ag(I) complexes were less

active than their Au(I) analogs; in the MDA-MB-231 line, they showed better performance than cisplatin.[15,27]
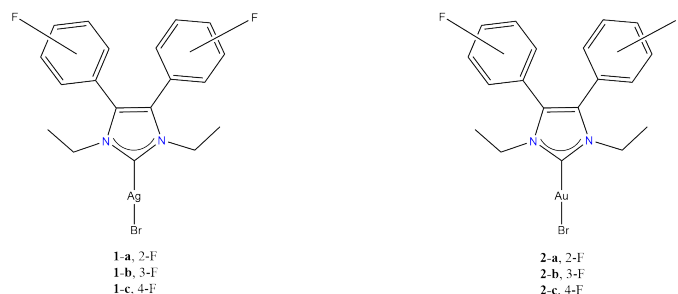
FIGURE 1.10: Ag(I) and Au(I) complexes derived from 4,5-diarylimidazole.[15]

Complex	MCF-7	MDA-MB-231	HT-29
1-a	3.4±0.7	3.6±0.2	7.5±0.5
1-b	3.5±0.1	4.1±0.7	7.4±0.8
1-c	3.9±0.2	3.5±0.3	4.4±0.1
2-a	0.80±0.06	1.7±0.9	3.3±1.0
2-b	3.1±0.1	6.4±0.1	4.2±0.3
2-c	1.1±0.3	3.9±0.1	2.3±0.1

TABLE 1.2: Cytotoxicity IC_{50} (μM) values against MCF-7, MDA-MB-231 and HT-29 by Ag(I) and Au(I) complexes.[15]

The 4,5-dicholorimidazole based Ag(I)-NHC compounds were the first to report anticancer activity, Youngs and coworkers developed them. Compounds in figure 1.11 were evaluated for *in vitro* antitumor activity against the cancer cell lines OVCAR-3 (ovarian), MB157 (breast), and HeLa (cervical). IC_{50}, the concentration at which 50% of cell growth is inhibited compared to a control cisplatin and $AgNO_3$. Cisplatin shows good activity against ovarian cancer cells with $IC_{50} = 12\mu M$, compared to $IC_{50} = 20 - 25\mu M$ from the silver complexes. Compounds $3 - a, b, c$ show ineffectiveness against the HeLa cell line $IC_{50} > 200\mu M$. Nevertheless, the silver compounds were most active against MB157 with IC_{50} values of $8\mu M$, $20\mu M$, and $10\mu M$ for $3 - a, b, c$ compounds respectively, compared to $IC_{50} = 25\mu M$ for cisplatin.[26] Considering the good result, an *in vivo* xenograft model study was developed utilizing OVCAR-3 and 3-a. OVCAR-3 cells were injected subcutaneously into the back of nude mice. After tumor growth became visible, compound 3-a was injected at the tumor location. According to the pathological studies, significant tumor cell death was observed while no ill effects to the major organs of the mice were detected.
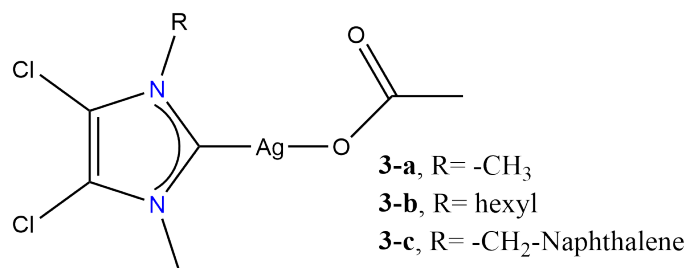
FIGURE 1.11: Structures of Ag(I)-NHC complexes synthesized by Youngs and coworkers.[26]

1.2 Cancer

1.2.1 Definition

Cancer is a large group of diseases in which cells of any tissue grow and multiply uncontrollably; threatening adjoining body parts. Cancer can start in any part of the body, in which the natural process starts with cell growth and cell division for new cells as the organism requires. Then, cells grow old or damaged, so they die (apoptosis), and new cells take their place.

When damaged or abnormal cells grow and multiply when they should have died. They may invade other parts of the body by forming lumps of tissue. Considering the invasion of other organs, there are two main types of cancers. Cancerous tumors can spread to other organs/tissues, traveling to different parts of the body to form new tumors (metastasis). Benign tumors do not invade other tissues; however, they can be large and life-threatening.[28,29]

1.2.2 Types

There are more than 100 types of cancers. Each cancer is named under the tissue or organ in which it is formed. Then, prostate cancer starts in the prostate, and breast cancer starts in the breast. Cancers developed in a specific organ or tissue and migrated to other parts of the body are called metastatic cancer. For example, cancer formed in the breast and produces a metastatic tumor in the lungs is named metastatic breast cancer, not lung cancer.[28]

1.2.3   World incidence and mortality

According to the World Health Organization (WHO), cancer is one of the most important causes of death worldwide, which produced almost 10 million deaths in 2020, or nearly 6 in 10 deaths. Also, the most common cancers are breast, lung, colon and rectum, and prostate cancers. According to WHO, breast (2 261 419), lung (2 206 771), colorectum (1 931 590), prostate (1 414 259), and stomach (1 089 103) cancers were the most diagnosed in 2020. Furthermore, lung (1 796 144), colorectum (935 173), liver (830 180), stomach (768 793), and breast (684 996) cancers produced more deaths in 2020.[4] In table 1.3, we can compare the incidence and mortality of the most common cancers.

Cancer	Incidence	Mortality
Lung	2 206 771	1 796 144
Colorectum	1 931 590	935 173
Prostate	1 414 259	375 304
Stomach	1 089 103	768 793
Liver	905 677	830 180
Oesophagus	604 100	544 076
Pancreas	495 773	466 003
Total	**8 647 273**	**5 715 673**

TABLE 1.3: Estimated number of incidences and mortality of the most common cancers (both sex, all ages)[4]

In table 1.4, we can compare the different values of incidence and mortality of cancer between world regions. It is important to consider that regions such as Asia, Europe, and North America could have higher values due to population size. Nevertheless, there are countries where no data on cancer is collected. Also, regions such as Africa, Latin America, and the Caribbean present high values due to lake of efficient early diagnosis of cancer.[3,4]

In Ecuador according to table 1.5, the cancers with high incidence and mortality are breast, prostate, stomach, colon, thyroid, cervix uteri, non-Hodgkin lymphoma, leukemia, and lung and liver cancers.[2]

Region	Incidence	Mortality
Asia	9 503 710	5 809 431
Europe	4 398 443	1 955 231
North America	2 556 862	699 274
Latin America and Caribbean	1 470 274	713 414
Africa	1 109 209	711 429
Oceania	254 291	69 354
Total	**19 292 789**	**9 958 133**

TABLE 1.4: Estimated number of incidences and mortality in different regions of the world (both sex, all ages)[4]

Cancer	Incidence	Mortality
Breast	3 563	1 056
Prostate	3 249	1 272
Stomach	2 472	2 007
Colon	1 795	984
Thyroid	1 685	232
Cervix uteri	1 534	813
Non-Hodgkin lymphoma	1 477	731
Leukaemia	1 199	897
Lung	1 185	1 069
Liver	915	880
Total	**19 074**	**9 941**

TABLE 1.5: Estimated number of incidences and mortality of the most common cancers in Ecuador (both sex, all ages)[2]

1.2.4 Treatments

With over more than 100 types of cancer; the number of treatments is high. However, not all treatments pass the required trials to be used by the general public. Nowadays, multiple treatments are being developed using actual technology that was not available before. There are three common treatments used for cancer treatments are[30,31]:

- Radiotherapy is a process in which high doses of radiation are used to kill cancer cells or reduce tumor size.

- Chemotherapy is the use of drugs to kill cancer cells.

- Surgery is a process in which surgeons try to extract the cancer tissue.

One of the most common alternatives in cancer treatment is the combination of two of the common treatments usually surgery combined with radiotherapy or

chemotherapy.

1.2.5   Drugs based on platinum

The discovery of platinum complexes as anticancer drugs is considered one of the known cases of serendipity. The first time it was synthesized was in 1945, and it was known as Peyrone's chloride. However, the biological application was tested in 1967 by Rosenberg.[32] For example, Cis- and trans-dichlorodiammineplatinum (II) have interesting biological properties, inducing filament formation and inhibiting cell 0division in *E. Coli*. Also, it was tested in tumor cells showing anti-tumor activity against Sarcoma 180 and Leukemia L 1210 in mice. With further tests, cisplatin was approved by the FDA in 1978 to be used against ovarian and testicular metastatic cancer.

In a willingness to improve the next generation of platinum drugs, the mechanism of action of cisplatin was studied. Then, the cisplatin mechanism of action can be explained in four steps: (i) cellular uptake, (ii) aquation or activation, (iii) DNA binding, and (iv) cellular processing of DNA lesions leading to cell death (figure 1.12).

In the cellular uptake, two possible pathways have been proposed, which are passive diffusion through the plasma membrane and active transport mediated by membrane proteins. Considering cisplatin's small size and square planar geometry, passive diffusion through the membrane can be considered the best path. On the other hand, other studies suggest active transport is the main mechanism of uptake. However, the best description of the uptaking of cisplatin is obtained when considering a combination of passive and active transport.

In the aquation or activation, cisplatin suffers a ligand substitution in which a chloride ligand is replaced with a water molecule. In DNA binding, the cisplatin with a water molecule (aquated cisplatin) enters the nucleus and can be replaced by a heterocyclic DNA base. Considering that the most nucleophilic sites of DNA are the N7 atoms of purine, guanine, and adenine; these are the preferred sites to be platinated. After this, the chloride suffers a substitution with a second guanine base, forming a cross-link on the DNA.
Finally, in cellular processing, there is evidence that shows the bending and unwinding of the double helix upon platination.[34]
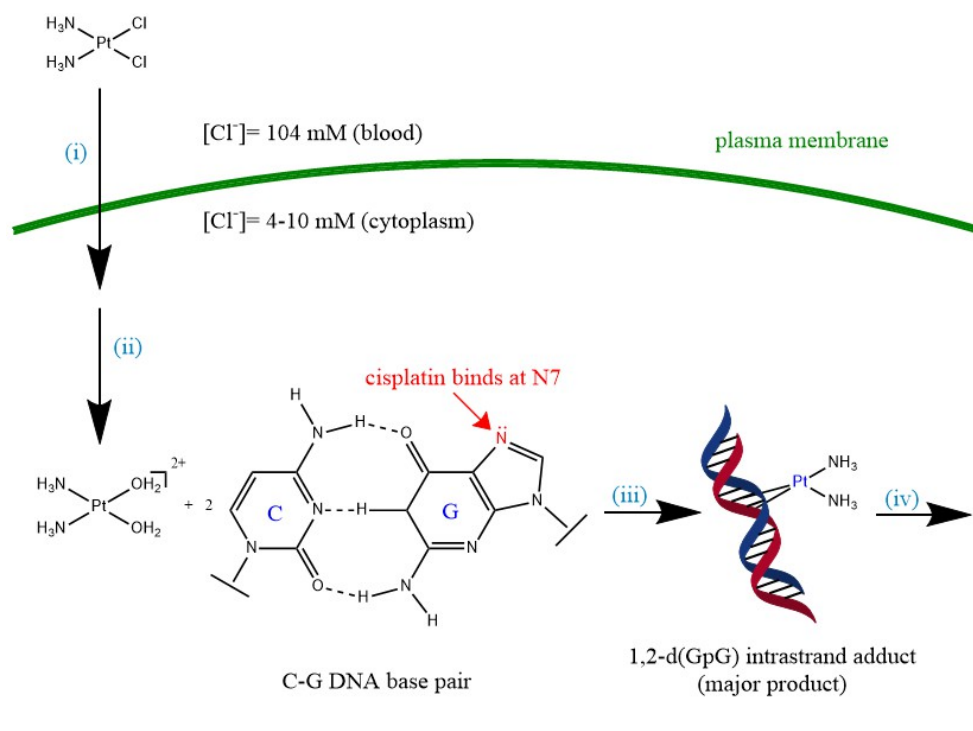
FIGURE 1.12: Illustration of the mechanism of action of cisplatin showing the following phases:(i) cellular uptake, (ii) aquation or activation, (iii) DNA binding, and (iv) cellular processing of DNA lesions leading to apoptosis.[33]

As cisplatin derives drugs are one of the main cancer treatments around the world, research around platinum-based drugs has been increasing over time. From all these efforts, three platinum-based drugs are approved worldwide for treating cancer: cisplatin, carboplatin, and oxaliplatin (figure 1.13-a). There are other three drugs approved in specific countries, nedaplatin, lobaplatin, and heptaplatin (figure 1.13-b).[35] However, platinum drugs such as cisplatin, oxaliplatin, and carboplatin present side effects, which are nausea, alopecia, anemia, infertility, nephrotoxicity, and ototoxicity, leading to the search for drugs with the same or higher activity and fewer side effects.

1.2.6 New metallodrugs

Metals play an important role in the human body, there are at least 10 metals that are considered essential for the body. Others are used in applications such as platinum drugs (cancer treatment), lithium (bipolar disorders), or silver (antimicrobials). Considering the necessity of new drugs, drug discovery, and development are focused on organometallic drugs, as they contain metals that have been proven to be good
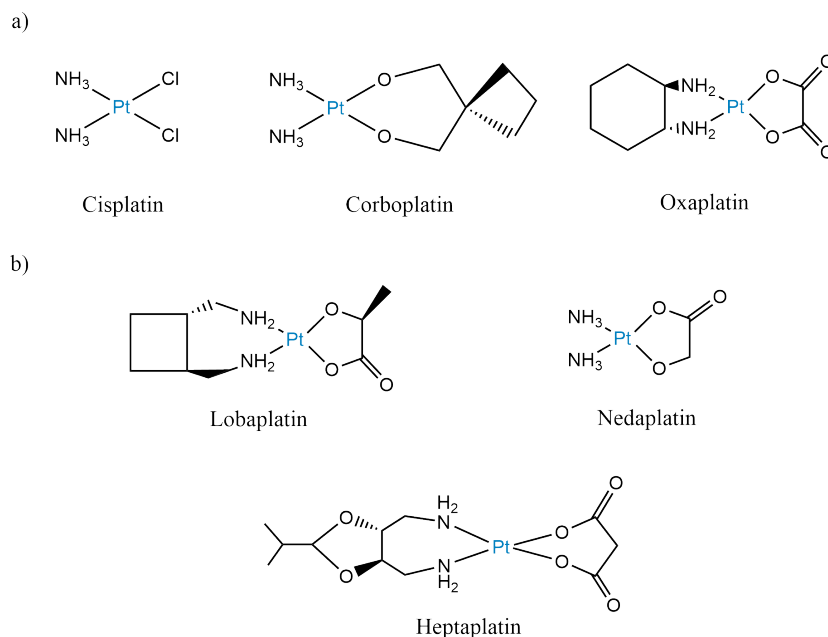
FIGURE 1.13: Platinum metallodrugs, a) Approved platinum metallo-
drugs, b) In clinical trials platinum metallodrugs.[35]

as cancer treatments, a variety of geometries, diverse stereochemistry, and most im-
portantly, ligands edition let control kinetic properties. Nowadays, there are the
required techniques to characterize, identify target sites, and elucidate the mecha-
nisms of action of these kinds of drugs. Many organometallic compounds used to
be applied as catalysts or biosensors (metallocenes, half-sandwich, carbenes, car-
bonyls); now, they are being applied in medicinal chemistry (figure 1.14).[15,36–38]

1.3   Problem Statement

For many years, scientists have been looking for new cancer treatments and new
ways to combat one of the most relevant diseases. Today, cisplatin is the lead-
ing treatment for multiple types of cancer because it limits and reduces cancer cell
growth. However, the use of cisplatin carries many secondary effects for the human
body in its battle with this disease.

Among the health problems that cisplatin can develop is related to the immune sys-
tem, which is severely compromised and leaves the body exposed to other illnesses
due to its low specificity towards cancer cells. Therefore, this work focuses on syn-
thesizing NHC Ag(I) complexes derived from theophylline, avoiding special con-
ditions such as inert atmosphere or high temperatures. By studying their effect on
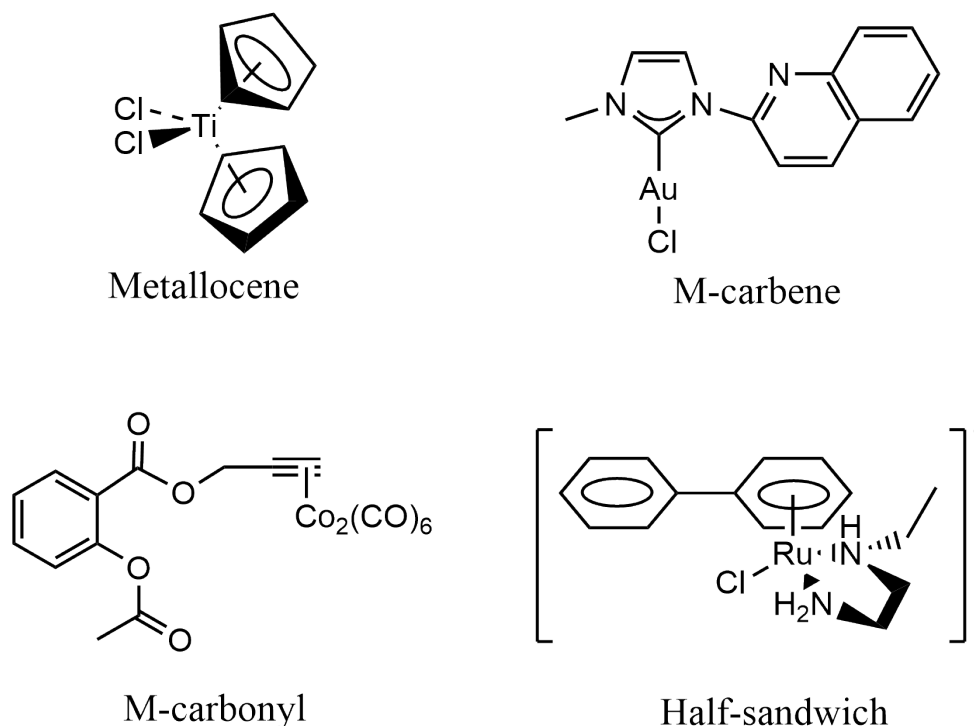
FIGURE 1.14: Organometallic compounds tested as anticancer compounds.[15,37,38]

different cancer cell lines and comparing them to a health cell line, the complexes' studies will be centered on their inhibition and selectivity towards cancer cells.

1.3.1 Objectives

General Objective

To synthesize and characterize a series of Ag(I) complexes, with N-heterocyclic carbenes (NHCs) derived from theophyllines. As well as evaluating their cytotoxic activity over different cancer cell lines.

Specific Objectives

- To obtain a series of NHCs derived from theophylline.

- To establish the reaction conditions for each synthetic step to obtain Ag(I) complexes.

- To purify and characterize the NHCs Ag(I) complexes by IR spectroscopy, HPLC, mass spectroscopy, and nuclear magnetic resonance (NMR).

- To analyze non-covalent interactions in the crystal lattice by X-ray spectroscopy.

- To perform primary screening of the complexes to identify those with cytotoxic activity.

- To conduct the crystallochemical analysis of the complex IIa by single-crystal X-ray diffraction.

Chapter 2

Methodology

The required reagents were acquired from Sigma Aldrich and used without further purification; the azolium salts were obtained according to the experimental procedure for synthesizing azolium salts by N-alkylation. Reactions were monitored using thin layer chromatography (TLC), using Alugram® SIL silica gel chromatofoils G/UV254 as stationary phase, the plates were developed using UV radiation (254nm) and iodine chamber. The NMR ^1H, $^{13}C\{1H\}$ and ^{19}F were obtained using Bruker AVANCE III HD 700 MHz for ^1H, $^{13}C\{1H\}$, HSQC, and HMBC; and JEOL GX300 spectrometer for ^{19}F, using TMS (tetramethylsilane) as intern reference and $DMSO - d_6$ and $Acetonitrile - d_3$ as solvents. The chemical shifts (δ) are expressed in parts per million (ppm) from the TMS and the coupling constants (J) in Hertz. For showing the signals multiplicity of ^1H NMR, it was used the following nomenclature: (s) simple signal, (d) double signal, (wss) wide single signal, and (m) multiple signals. Mass spectra were obtained from MStation using FAB^+ ion mode, and the signals are reported in m/z. High Performed Liquid Chromatography (HPLC) chromatograms were obtained using UV-Vis Diodes array Waters 2996 and Kinetex 5 μm EVO C18 100 as the column. For the IR spectrometers, it was used FT-IR NICOLET IS-50, Thermo Fisher Scientific. The single-crystal data was obtained through Bruker APEX-II CCD.

2.1 Synthesis and characterization of the compounds

2.1.1 General synthesis procedure for compounds IIa-e

A solution of Ag_2O (50mg, 0.2158mmol) and the corresponding azolium salt, Ia-c (50mg, 0.1282mmol), Id (50mg, 0.1225mmol), and Ie (50mg, 0.1082mmol) in acetonitrile or DMSO (3 mL) in constant agitation and darkness (protected with aluminum foil) overnight at room temperature (figure 2.1). Then, the solution was filtered with celite ® . The yielding of the compounds could not be obtained because of the instability of the complexes once the solvent is removed; therefore, it was not performed elemental analysis and yielding calculations.

2.1.2 Strategy for the synthesis of the complexes
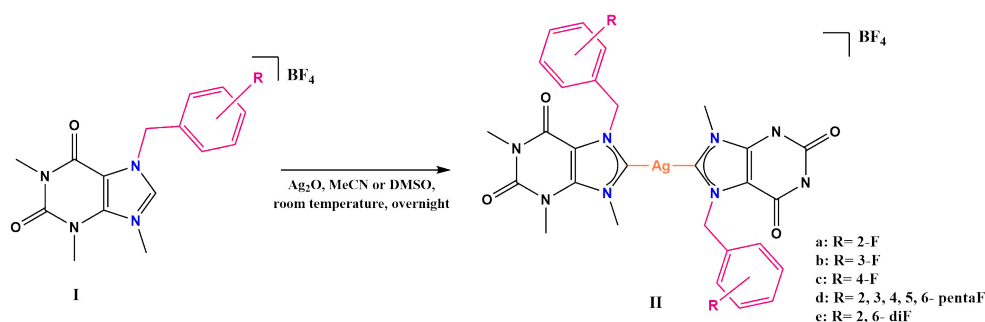
FIGURE 2.1: Strategy for the synthesis of NHC Ag (I) complexes (IIa-e)

2.1.3 Cytotoxic evaluation

The cell lines used at the biological tests laboratory in the "Instituto de Química" (I.Q.) at the Autonomous National University of Mexico (UNAM) belong to the Comprehensive Cancer Information from the U.S. Government (NCI), which were adapted to the culture medium RPMI-1640 added with bovine fetal serum (10%), a mixture of antibiotics-antimycotics at 10% and 2 mM glutamine. The doubling time of these lines is characterized. With it, the inoculum density that is deposited in each microwell was established, as shown in table 2.1.

Cell line	Organ of origin	Duplication time (h.)	cells/well
U-251	Nervous central system	25.4	7 500
PC-3	Prostate	28.7	7 500
HCT-15	Colon	18.1	10 000
MCF-7	Breast	25.6	5 000
SKLU-1	Lung	25.4	7 500

TABLE 2.1: Cytotoxicity IC_{50} (μM) values against MCF-7, MDA-MB-231 and HT-29 by Ag(I) and Au(I) complexes.(ref 38)

The cell lines adhere to the culture bottles and to harvest them, 1 mL of 0.05% trypsin-EDTA is added. As soon as the cells detach from the plastic substrate, 5-10 mL of culture medium is added to inactivate trypsin. The cells in suspension are deposited in conical tubes and centrifuged for 3 min. Once the cell package is formed, a culture medium is added to collect them. 50 μL of the inoculum is taken from the suspension and resuspended in 50 μL of trypan blue (vital dye), and the viability count is carried out in an automated Bio-Rad counter. Once the number of cells per mL has been determined, the inoculum is deposited in a 100 μL/well volume at cell density.

Each plate is inoculated with two triplicate cell lines and preincubated for 24 hours at $37^o C$ with an atmosphere of 5% CO_2 and 100% relative humidity, to promote stability. The concentration of 25 μM is tested for a primary compound screening. All samples are solubilized in dimethyl sulfoxide (DMSO) 100 times more concentrated than the concentration to be tested. Immediately after the preparation of the samples in solution and in the case of making curves concentration-response (5 dilutions are tested) add 100 μL, the volume being end of 200 μL well. The microplate is incubated again for 48 hours under the conditions above.

At the end of the incubation period of the compounds with the cells, these are precipitated (or fixed) *in situ* by adding $50\mu L$ of a 50% cold TCA solution, incubated at $4^o C$ for 1 hour. The supernatant is discarded and the plates are washed 5 times with deionized water and air-dried. The staining of the cells fixed to the substrate of the well is carried out with $100\mu L$ of a 0.4% solution of SRB and incubating for 30 minutes at room temperature. Unbound SRB is removed with 3 washes with 1% acetic acid and allowed to air dry. $100\mu L$ of a tris buffer are added to the stained plates and they are shaken for 10 minutes to favor the dissolution of the complex; OD is then measured in a microplate reader at a wavelength of 515 nm.

The data is processed by obtaining the average of the OD of the 3 wells/line treated with the compound (DO_t), the 3 wells treated with DMSO (DO_c), and 2 control wells, that is, those that do not have cells but do have a compound (DO_b). The % growth inhibition (%CI) is calculated with the following expression (equation 2.1):[27]

$$\%IC = 100 - \frac{100(DO_t - DO_b)}{DO_c - DO_b} \qquad (2.1)$$

Chapter 3

Results and Discussion

3.1 Synthesis and characterization of the compounds

3.1.1 Synthesis of Ag(I) NHC complexes IIa-e

The synthesis of Ag(I) NHC complexes IIa-e was done by cleaving the carbene carbon to the Ag atom (figure 2.1). The reaction of Ag_2O with the corresponding azolium salt Ia-e in acetonitrile or DMSO obtained the desired Ag (I) NHC complexes. The complexes IIa-e % yielding could not be determined due to the instability of the complexes once the solvent is removed.

3.1.2 Characterization of Ag(I) NHC complexes IIa-e

Complexes FT-IR spectra analysis

The samples for FT-IR ATR were obtained after filtration with celite and analyzed as liquid samples. All the complexes under investigation exhibit four distinct functional groups that are evident in the Fourier Transform Infrared (FT-IR) spectra (refer to Figure 3.1 and appendices A.1-A.4). These functional groups encompass carbonyl vibrations $C = O$ originating from amides, $C - N$ vibrations arising from tertiary amines, $C = N$ vibrations associated with imines, and $C - F$ vibrations. However, it is worth noting that the characteristic signal of $C - H$ out-of-plane bending vibrations, which indicates the degree and position of substitution in the aromatic ring, cannot be detected in these specific complexes. Furthermore, the spectral region of $2000 - 1667 \ cm^{-1}$, which is typically informative for determining the position substitution in substituted benzoic compounds, does not clearly exhibit the corresponding signals for each complex. Considering that infrared spectroscopy is a qualitative analysis method that allows for detecting major functional groups,

it is not surprising that complete information about the complexes cannot be obtained solely through this technique. Therefore, additional investigations employing complementary techniques such as nuclear magnetic resonance (NMR), high-performance liquid chromatography (HPLC), fast atomic bombardment (FAB), and single-crystal X-ray analysis may be necessary to obtain a comprehensive understanding of these complexes. For the purpose of this discussion, one representative complex (complex IIa, as depicted in Figure 3.1) will be analyzed due to the similarity observed in the FT-IR spectra among all the complexes (refer to appendices A.1-A.4).

Two significant stretching signals associated with $C = O$ vibrations are observed within the wavenumber range of $1709.11 - 1708.11 \, cm^{-1}$ and $1670.87 - 1668.97 \, cm^{-1}$. Generally, the carbonyl bands (corresponding to $C = O$ stretching) are located between $1700 - 1640 \, cm^{-1}$. These bands predominantly arise from carbonyl groups present in amides. The signals observed at $1670.87 - 1668.97 \, cm^{-1}$ are attributed to a carbonyl group flanked by two neighboring nitrogen atoms. The presence of these nitrogen atoms affects the shielding of the signal, resulting in a lower wavenumber than the signals at $1709.11 - 1708.11 \, cm^{-1}$, where only one neighboring nitrogen atom is present.

The stretching signal associated with $C - N$ vibrations can be observed within the range of $1350 - 1000 \, cm^{-1}$, and it appears at $1077.85 - 1075.58 \, cm^{-1}$ in the spectrum corresponding to tertiary amines.

The $C - F$ stretching signal is typically found within the $1400 - 1000 \, cm^{-1}$ range. However, due to the influence of the aromatic ring to which the fluorine atom is attached, the signals are observed within the range of $997.01 - 995.12 \, cm^{-1}$.

Finally, the stretching vibrations associated with $C = N$ in imines are of particular significance as this part of the molecule is bonded to the silver atom. In general, the imine signals are located within the range of $1500 - 1350 \, cm^{-1}$ [39], which encompasses the Ag(I)-NHC (N-Heterocyclic Carbene) interaction. In the spectrum, the peak corresponding to this signal is observed within the range of $1536.40 - 1524.20 \, cm^{-1}$.
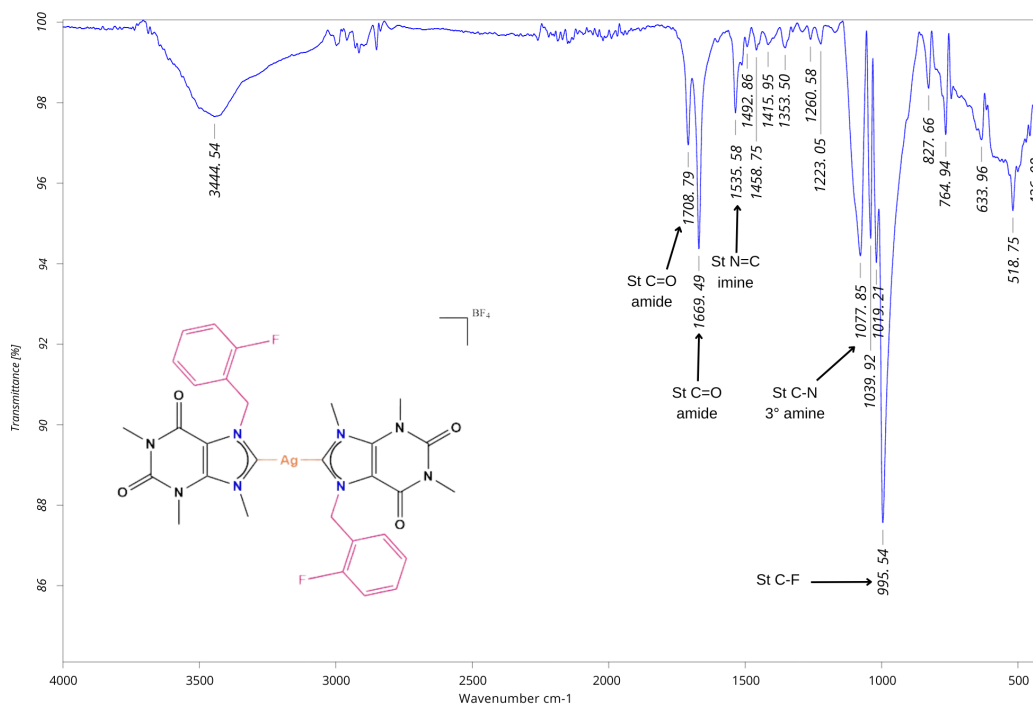
FIGURE 3.1: FT-IR spectrum of complex IIa, showing the most important stretching bands for the molecule

^1H **NMR spectrum**

For all NMR analysis the reactions were carried out in deuterated solvent ($DMSO - d_6$), filtered with celite and directly performed the NMR analysis. The first signal that we can analyze to consider that the complex has been obtained for complex IIa is observed in the ^1H NMR (figure 3.2). The signal for the fragment $NH\mathbf{H}N$ is not observed. Also, another important group signal is from the fragment $-C\mathbf{H}_2-$, which is found at 5.71ppm. The rest of the signals are assigned in Figure 3.2 and analyzed in Table 3.1.

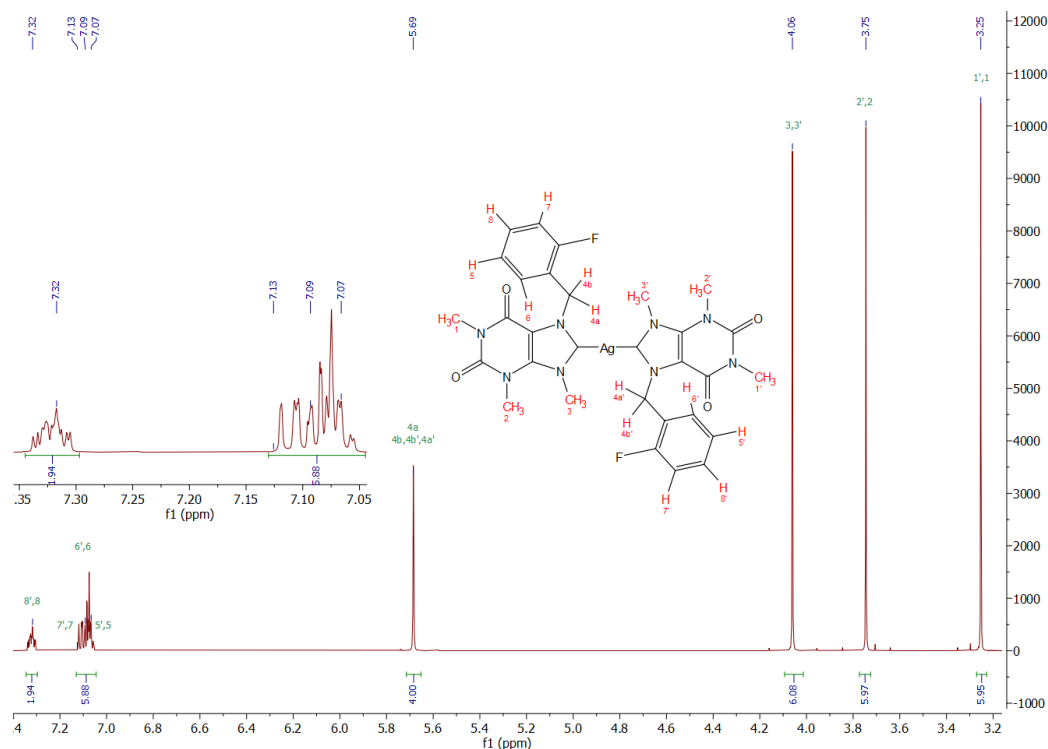FIGURE 3.2: ^1H NMR spectrum (700 MHz, $acetonitrile - d_3$) of the compound IIa

Peak	Experimental value (ppm)	Theoretical value (ppm)	Integral	Multiplicity	Number of H around
1	3.25	2.2-2.9	6	singlet	0
2	3.75	2.2-2.9	6	singlet	0
3	4.06	3.77-4.27	6	singlet	0
4	5.69	5.68-5.85	4	singlet	0
5	7.07	6.5-8.0	2	multiplet	2
6	7.09	6.5-8.0	2	multiplet	1
7	7.13	6.5-8.0	2	multiplet	1
8	7.32	6.5-8.0	2	multiplet	2

TABLE 3.1: Analysis of the peaks for ^1H NMR spectrum of compound IIa

Considering that the fragment from the theophylline is presented in all the complexes IIa-e the same analysis can be obtained for complexes IIb-e, the analysis tables and spectra can be found in the appendices A.1, A.5, A.2, A.6, A.3, A.7, A.4, and A.8.

However, an important part of being analyzed is the aromatic range from all the complexes because those signals are the ones that differentiate one complex from the other. We can distinguish three main cases in the aromatic region. In figure 3.3,

we can analyze the aromatic range for the complexes between 7.75-6.75 ppm. In figure 3.3a-c, we find the aromatic region of monosubstituted compounds IIa, IIb, and IIc.

In figure 3.3a, we observe two main signals, and in each, there is the superposition of two signals. Signals 1 and 2 are the more shielded, considering the effect of fluor over signals 3 and 4, which are downfield because of the deshielding effect of the fluor.

In figure 3.3a, which corresponds to complex IIa, we observe two main signals in each, there is the superposition of two signals. Signals 1 and 2 are the more shielded, considering the effect of fluor over signals 3 and 4, which are downfield because of the deshielding effect of the fluor.

The spectrum that corresponds to complex IIb is in the figure 3.3b. Here we have three signals, that vary due to the *-meta* Fluor substitution. Signal 4 is the more deshielded due to the effect of the fluor and the near oxygen from the amide near to the atoms. Meanwhile, signal 3 feels the effect of the neighbor fluor and signal 2 feels the effect of the near oxygen.

In figure 3.3a corresponds to complex IIc, the aromatic part of this complex is symmetric due to the *-para* fluor substitution, which explains the presence of two signals. Complex IIe is pentasubstituted, meaning that there should not be any signal in the aromatic region, the signal observed in figure 3.3d is part of impurities from the ligand that remains in the solution.

Finally, the spectrum in figure 3.3e corresponds to the complex IIe. This spectrum is easily differentiated from the others due to the integrations of hydrogens because this spectrum possesses one less hydrogen than the monosubstituted complexes. Also, the positions of the fluor atoms provide symmetry, generating two signals in the spectrum.
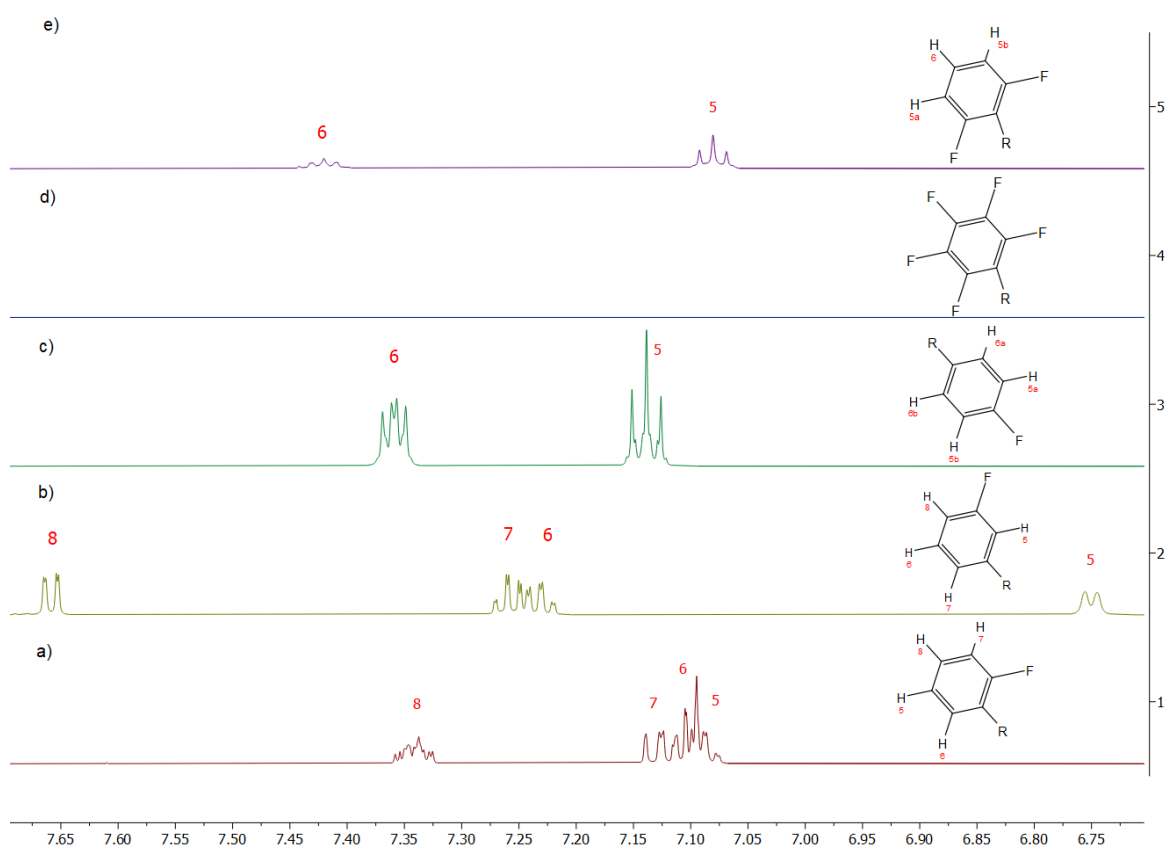
FIGURE 3.3: ^1H NMR spectrum (700 *MHz, acetonitrile* $-d_3$ and $DMSO-d_6$) of the compounds IIa-e; a) Complex IIa; b) Complex IIb; c) Complex IIc; d) Complex IId; and, e) Complex IIe.

$^{13}C\{^1H\}$ NMR spectrum of IIa complex

In the spectrum $^{13}C\{^1H\}$ from the IIa complex, the number of signals is directly related to the structure of the complex (figure 3.4). The most relevant signal corresponds to the carbene-carbon ($Ag-C_{carbene}$), which is present at 188.90ppm. This signal confirms the coordination between the Ag(I) and the carbene-carbon from the ligands. In the region from 115 to 165ppm, we can find the aromatic signals and the ones from the amide carbons. For signal 14, it appears twice since the ligands are not exactly symmetrical and the position of the fluor atoms in each ligand is not completely symmetrical from one to the other or the effect of ^{19}F coupling as the ^{13}C NMR is decoupled from ^1H but not from ^{19}F. The rest of the signals are assigned in figure 3.4. The complexes IIb-e have signals similar to the ones described for complex IIa, and the assignation can be found in the appendixes A.15, A.16, A.17 and A.18.
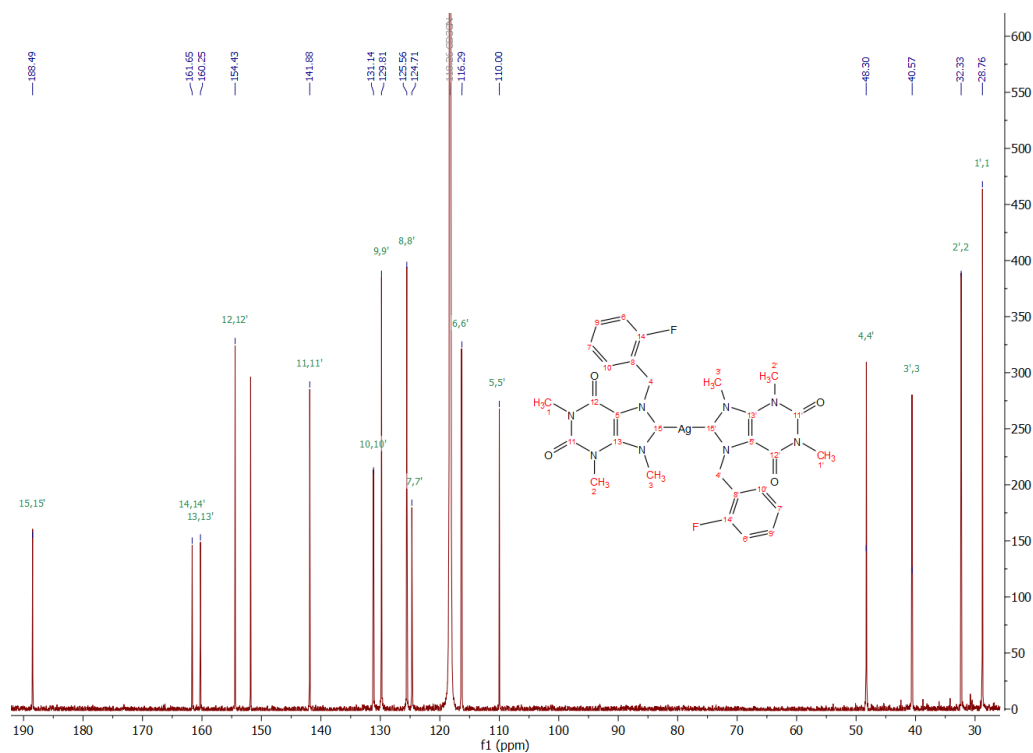
FIGURE 3.4: $^{13}C\{^{1}H\}$ NMR spectrum (176 MHz, *acetonitrile* $-d_3$) of compound IIa.

^{19}F **NMR spectrum of IIa complex**

In the spectrum ^{19}F from the IIa complex (figure 3.5), we can observe two signals that are part of the aromatic fragment of the complex. The signal at -151 ppm corresponds to the counter ion of the complex (BF_4). The second signal at -118 ppm corresponds to the aromatic ring's fluor in the $-ortho$ position. The symmetry of the leads to the presence of just one signal. The same effect is observed in all mono-fluorated compounds. The spectra for complexes IIb and IIc are in appendixes A.19 and A.20, respectively.

Complex IId (fig 3.6) presents four signals corresponding to the penta-fluorated aromatic rings. Three signals correspond to the complex's aromatic part, and the fourth one corresponds to the complex's counter ion (BF_4). Each signal is assigned considering the F-F coupling effect in the aromatic ring.

Complex IIe (fig 3.7) shows two signals corresponding to the counter ion and the symmetric di-fluorated aromatic part of the complex.[40]
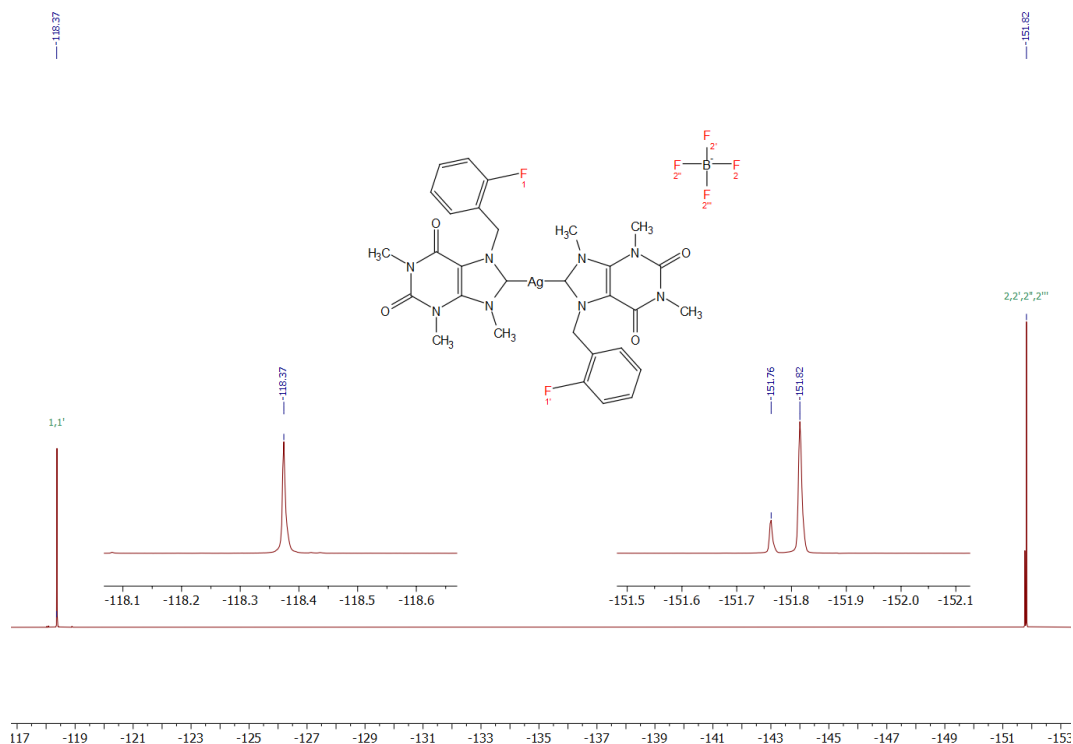
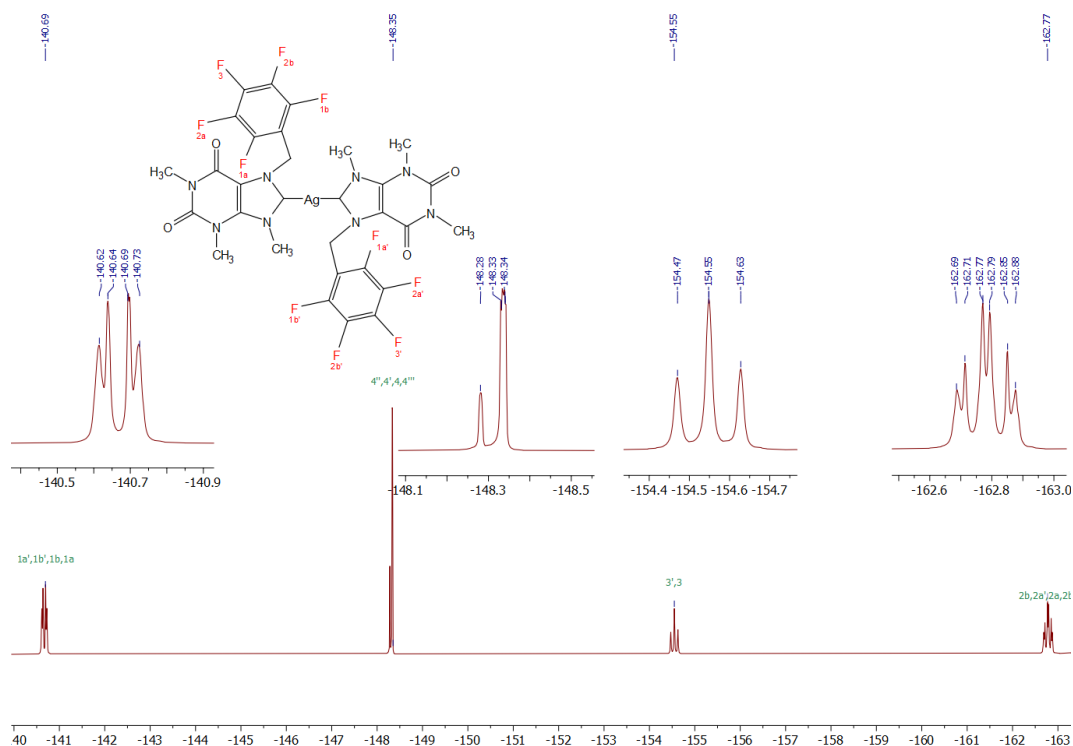FIGURE 3.5: $^{19}F\{^1H\}$ NMR spectrum (282 MHz, $acetonitrile - d_3$) of compound IIa.

FIGURE 3.6: $^{19}F\{^1H\}$ NMR spectrum (282 MHz, $DMSO - d_3$) of compound IId. The signals 4, 4', 4'', and 4''' correspond to the counter ion BF_4

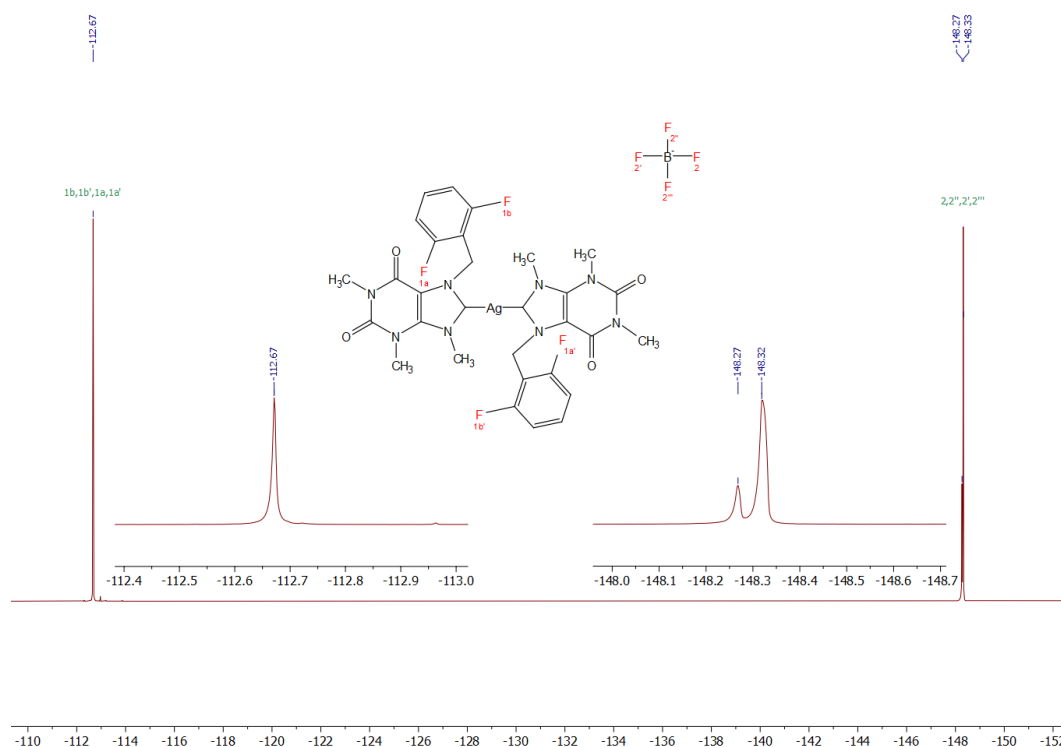FIGURE 3.7: $^{19}F\{^1H\}$ NMR spectrum (282 MHz, $DMSO-d_3$) of compound IIe.

3.1.3 Heteronuclear Single Quantum Coherence (HSQC) and Heteronuclear Multiple Bond Correlation (HMBC)

HSQC and HMBC provide further information regarding the structure of the molecule. Specifically, HSQC shows the proton-carbon single-bond correlations. HSQWC helps to elucidate the structure of our complexes. Figure 3.8 shows the interaction of each C-H in the ^1H and ^{13}C NMR spectra. The use of HSQC is helpful for the assignation of the signal in the aromatic region in each complex.

The HMBC helps us observe the correlations between carbons and protons that are separated by two, three, and sometimes in conjugated systems, four bonds. HMBC signals for complex IIa (figure 3.9) give coherent signals from hydrogen and carbon atoms separated by a single bond or multiple bonds. In each figure, the C-H interaction for all complexes is marked. The HSQC and HMBC spectra for all compounds can be found in the annexes. Figures A.21 and A.25 for compound IIb; figures A.22 and A.26 for compound IIc; figures A.23 and A.27 for compound IId; and, figures A.24 and A.28 for compound IIe.
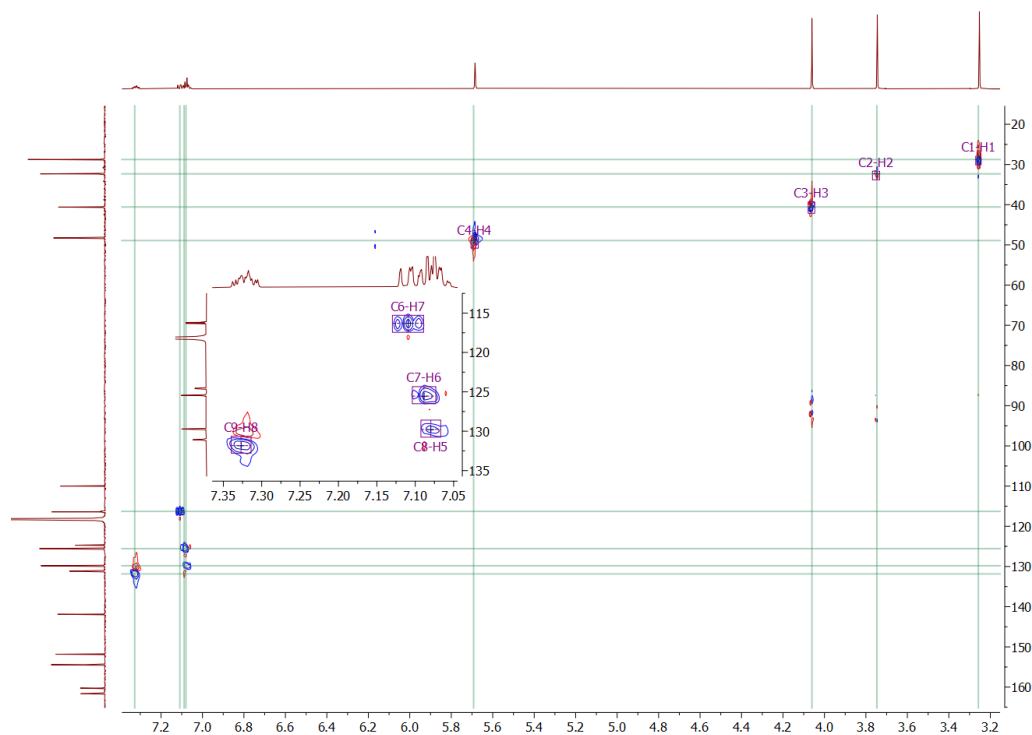
FIGURE 3.8: HSQC spectrum ($^1H = 700$ *MHz and* $^{13}C = 176$ *MHz,* *acetonitrile* $- d_3$) of compound IIa (an expanded form of the aromatic zone is shown in the box inset).

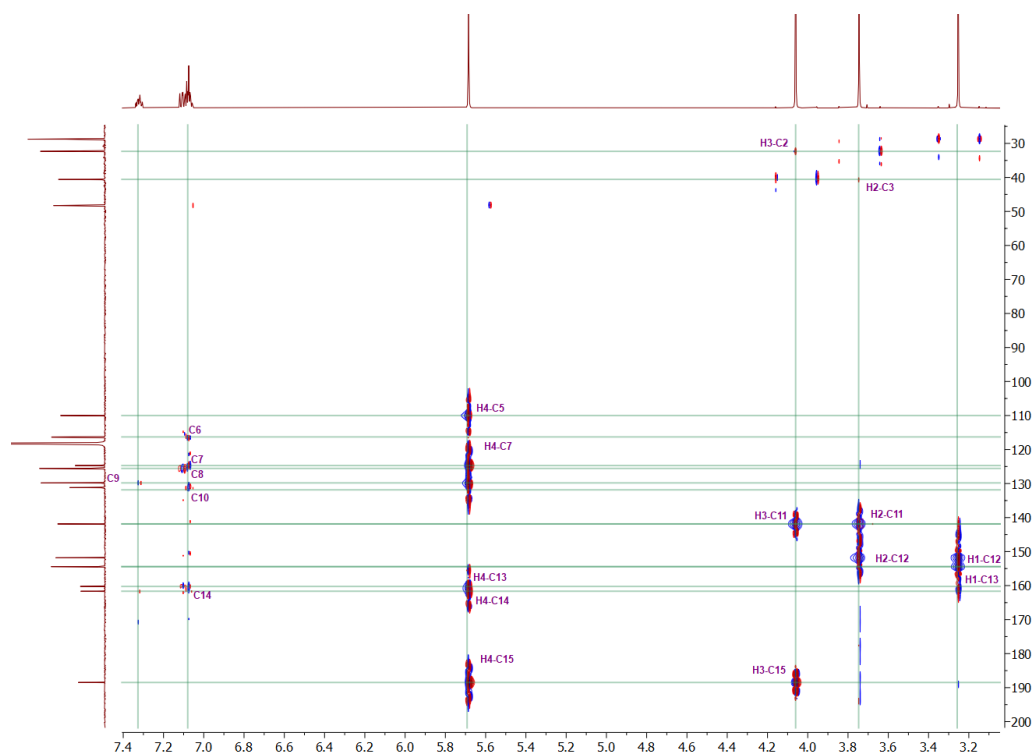FIGURE 3.9: HMBC spectrum ($^1H = 700$ *MHz and* $^{13}C = 176$ *MHz,* *acetonitrile* $- d_3$) of compound IIa.

Mass spectra of complexes IIa-e

The samples were filtrated with celite and sent as liquid samples. In the mass spectrum (figure 3.10), we can appreciate the molecular ion $[M]^+$ of the compound in 711 m/z, corresponding to the complex IIa's mass. Complexes IIb and IIc, have the same molecular weight as complex IIa, therefore, they will have the same mass (appendices A.9, A.10). Complexes IId-e have different fluorination degrees, meaning that they will present different mass values. Specifically, 749 m/z for complex IIe (figure 3.11); and 857 m/z for complex IId (figure 3.12).
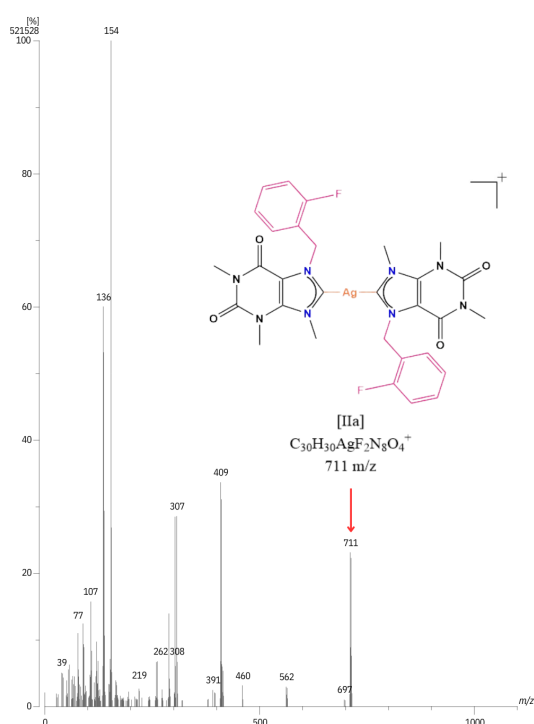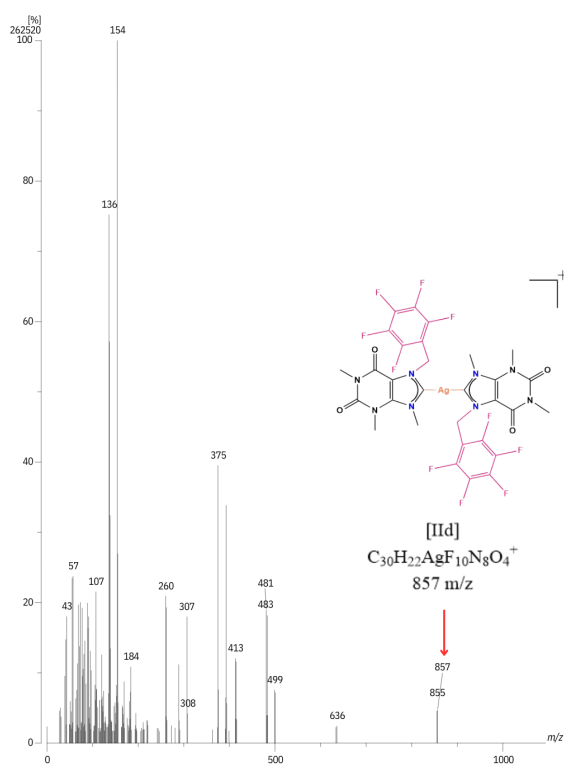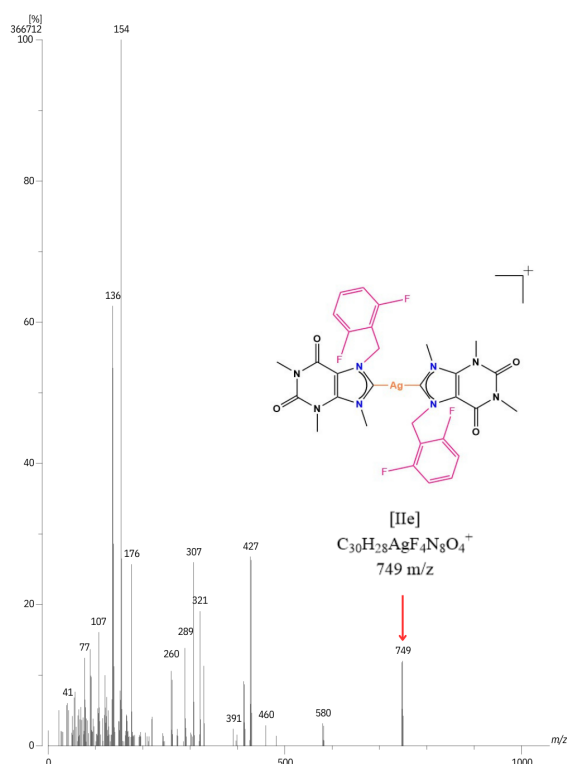

FIGURE 3.10: FAB^+ mass spectrum of complexes IIa.

FIGURE 3.11: FAB^+ mass spectrum of complexes IId.

FIGURE 3.12: FAB^+ mass spectrum of complexes IIe.

HPLC chromatograms of IIa-e complex

The samples for HPLC were obtained after filtration with celite and analyzed and brought to 1M concentration as liquid samples. HPLC chromatograms of the complexes present peaks from 12 to 20 min at 254nm. Figure 3.13 shows the HPLC chromatogram of complex IIa. Considering the product's structure, it is possible to establish that the peak at 13.994 min (peak 4) belongs to the Ag(I) NHC complex IIa. As well as complex IIa the other complexes IIb-e present a prominent peak between 13.994 and 15.347 min. This peak is of great help in analyzing the conversion percentage of the synthesis, which is essential considering that we cannot have the yielding of the reaction due to the instability of the compounds. Regarding the UV-Vis profiles complexes IIa-b, they present similar profiles with two peaks; one is around 234nm, and the second is around 198nm. The HPLC chromatograms and UV-Vis profiles of complexes IIb-e can be found in appendices A.11, A.12, A.13, and A.14. The chromatograms present the most intense peak in each one, representing the majority fraction according to the peak area 97.62%, 94.68%, 96.15%, 97.57%, and 97.95% for each complex IIa-e, respectively.
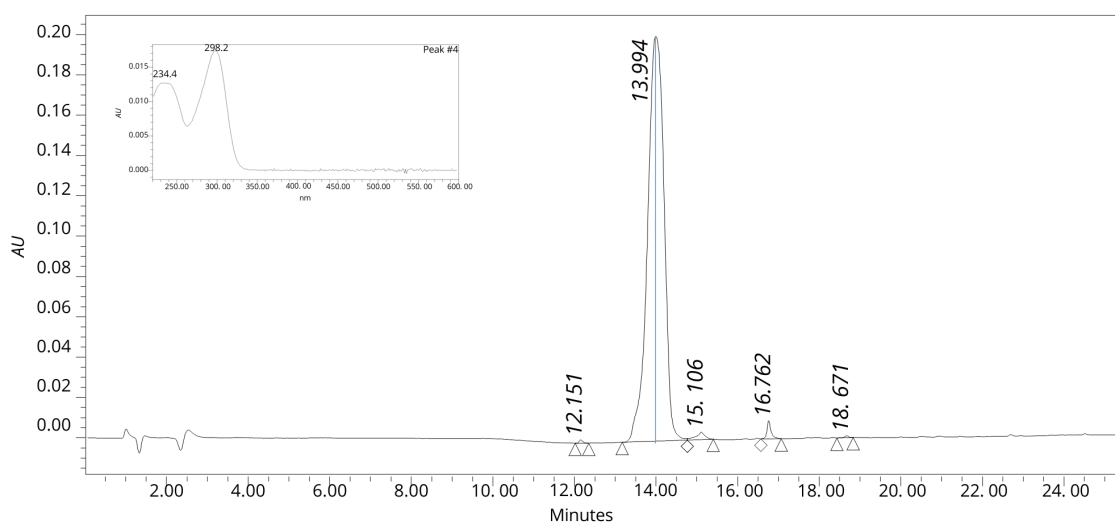

FIGURE 3.13: HPLC chromatogram of IIa complex. RP-HPLC: [linear gradient ACN/H_2O (5:95) to (100:0) over 20 min].

3.1.4 Crystallochemical analysis of the complex IIa

The crystal was obtained using diffusion with DMSO as solvent and diethyl ether as carrier. The molecular structure of complex IIa was determined unequivocally using single-crystal X-ray diffraction. The crystallographic data of collection and refinement are shown in Table 3.2. All data will be compared to the complex synthesized by Hameury[41] that is labeled as complex A ($C_{12}H_{20}AgClN_4O_2$), this complex processes similar features to complex IIa, and it will be helpful to compare the most important characteristics of the complex's structure.

The single-crystal of the complex IIa was obtained using slow diffusion of diethyl ether in a concentrated solution of the complex using acetonitrile as solvent.
The crystalline system for the complex IIa is monoclinic with a $C2/c$ space group, and it contains four molecules in the unitary cell (Z=4), the same information is obtained for complex A.
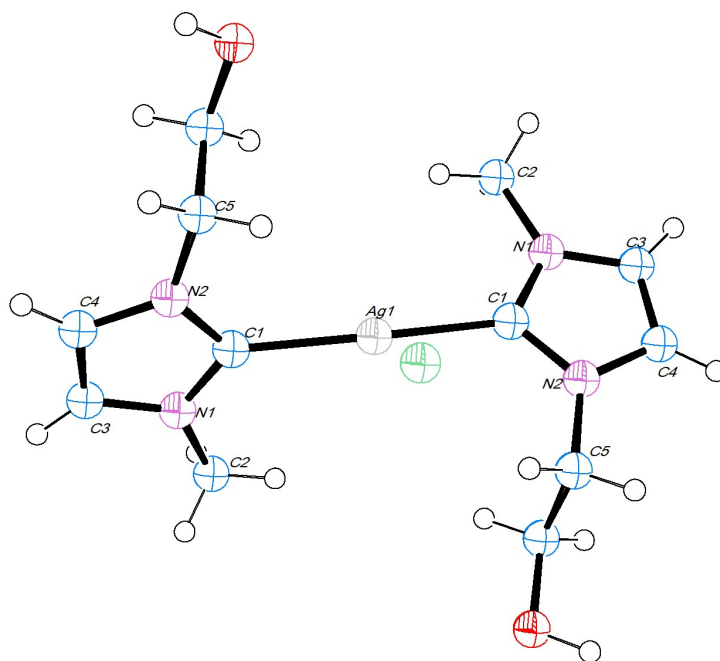
	Complex IIa
Crystal data	
Empirical Formula	$C_{30}H_{30}AgBF_6N_8O_4$
Formula Weight (M_r)	799.30
Crystal system, space group	Monoclinic, $C2/c$
Temperature (K)	100(2)
a, b, c (Å)	27.737(2), 8.2695(8), 13.7661(13)
α, β, γ (°)	90, 102.842(5), 90
Volume (Å)	3078.6(5)
Z	4
Radiation type	CuK/a
Absorption coefficient μ (mm^{-1})	6.048
Crystal size (mm)	0.233 x 0.130 x 0.052
Data collection	
Diffractometer	Bruker APEX-II CCD
Absorption correction	Multi-scan
Transmission (T_{min}, T_{max})	0.5065, 0.7531
No. of measured, independent, and observed $[I > 2\sigma(I)]$ reflections	6680, 2483, 1443
R_{int}	0.1205
$(sin\,\theta/\lambda)_{max}$(Å^{-1})	0.605
Refinement	
$R[F^2 > 2\sigma(F^2)]$, $wR(F^2)$, S	0.091, 0.251, 0.99
No. of reflections	2483
No. of parameters	224
No. of restrains	0
H-atom treatment	H-atom parameters constrained
$\Delta\rho_{max}$, $\Delta\rho_{min}$ (e Å^{-3})	2.042, -1.939

TABLE 3.2: Experimental details for complex IIa. Computer programs: *APEX2* (Bruker, 2012), *SAINT* (Bruker, 2012), *SHELXS-97* (Sheldrick 2008), *SHELXL-2018/3* (Sheldrick, 2018), *SHELXTL* (Sheldrick, 2013)

Figure 3.16 and 3.17 show a linear geometry slightly distorted around the metallic center in both complexes. The NHC ligands are coordinated to the Ag(I) atom. The bond distance for Ag(I)-NHC is 2.090(10) Å in complex IIa (Figure 3.14a), which is common for this kind of compound as we can see in complex A with a value of 2.083(3) Å (Table 3.4) (Figure 3.14b). In figure 3.16, we can see a lateral view of the complexes. Here, it is a palpable fact that complex IIa (figure 3.15a) and complex A (figure 3.15b) are not completely linear. The most relevant bond distances and angles are shown in table 3.3 for complex IIa and table 3.4 for complex A.
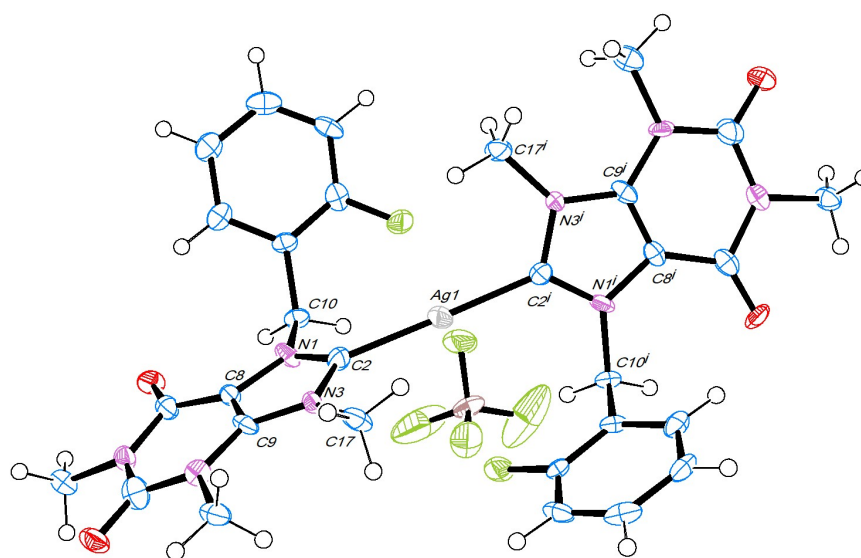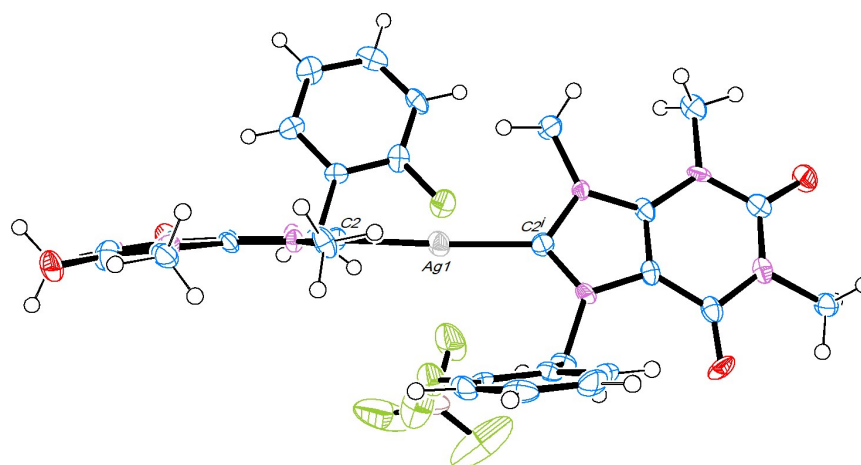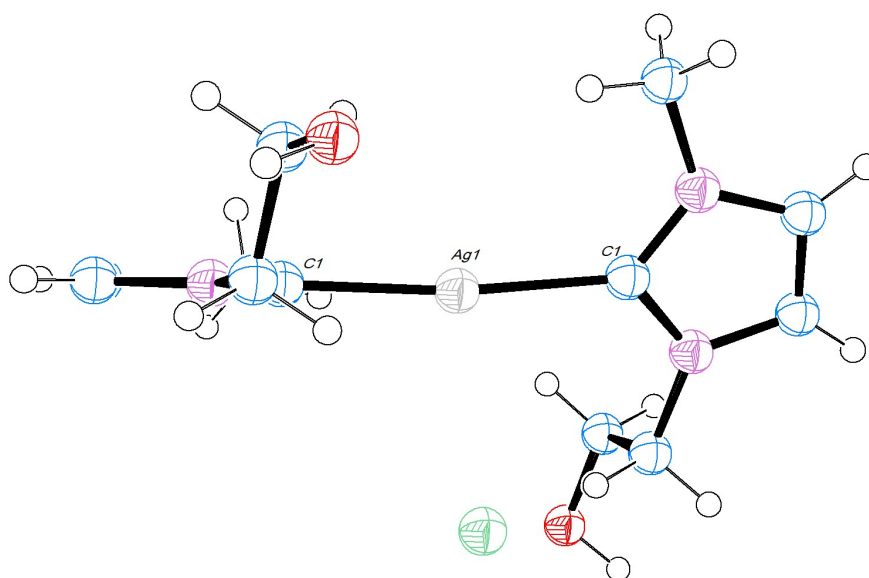
(A) Complex IIa

(B) Complex A

FIGURE 3.14: Frontal view of the molecular structure of complex IIa (A)
and complex A (B). The ellipsoids are represented at 50% of probability

(A) Complex IIa

(B) Complex A

FIGURE 3.15: Lateral view of the molecular structure of complex IIa (A) and complex A (B). The ellipsoids are represented at 50% of probability

	bond length (Å)		angle (°)
Ag(1)-C(2)	2.090(10)	C(2)-Ag(1)-C(2)*	177.4(7)
Ag(1)-C(2)*	2.090(10)	C(2)-N(1)-C(8)	110.7(10)
F(1)-C(12)	1.367(13)	C(2)-N(1)-C(10)	121.8(9)
O(1)-C(5)	1.219(15)	C(2)-N(3)-C(17)	120.9(9)
O(2)-C(7)	1.218(14)	C(5)-N(4)-C(9)	118.5(11)
N(1)-C(2)	1.326(14)	C(5)-N(6)-C(7)	128.0(10)
N(1)-C(8)	1.392(14)	N(1)-C(2)-N(3)	105.5(9)
N(1)-C(10)	1.485(14)	N(1)-C(2)-Ag(1)	130.5(9)
N(3)-C(2)	1.398(15)	N(3)-C(2)-Ag(1)	124.0(8)
N(3)-C(17)	1.468(14)	O(1)-C(5)-N(6)	122.4(11)
N(4)-C(5)	1.387(15)	N(6)-C(5)-N(4)	116.8(12)
N(6)-C(5)	1.380(17)	O(2)-C(7)-C(8)	127.9(12)
N(6)-C(7)	1.412(15)	N(6)-C(7)-C(8)	110.0(11)
C(10)-C(11)	1.516(16)	C(8)-C(9)-N(3)	110.1(11)
		F(1)-C(12)-C(11)	117.5(12)
		N(1)-C(10)-C(11)	112.2(9)

TABLE 3.3: Selected geometric parameters, bond length and angle (Å, °) complex IIa

	bond length (Å)		angle (°)
Ag(1)-C(1)	2.086(3)	C(1)-Ag(1)-C(1)*	172.27(15)
Ag(1)-C(2)	2.086(3)	N(2)-C(1)-Ag(1)	128.3(2)
C(1)-N(2)	1.349(4)	N(1)-C(1)-Ag(1)	127.5(2)
C(1)-N(1)	1.352(4)	C(4)-C(3)-N(1)	106.9(3)
C(2)-N(1)	1.456(4)	C(3)-C(4)-N(2)	106.7(3)
C(3)-C(4)	1.332(5)		
C(3)-N(1)	1.381(4)		
C(4)-N(2)	1.384(4)		
C(5)-N(2)	1.464(4)		

TABLE 3.4: Selected geometric parameters, bond length and angle (Å, °) complex A

In figure 3.16, we can see a lateral view of the complexes. Here, it is evident that the ligands are not completely symmetric in figures 3.16a and 3.16b, the angle between the azolium part of the complexes is not 90 degrees. Then, in figures 3.17a and 3.17b, we measure the angle between two planes form with N(1)-C(2)-N(3) and N(1)*-C(2)*-N(3)* in complex IIa, and N(1)-Ag(1)-N(2) and N(1)*-Ag(1)*-N(2)* in complex A. For complex IIa and complex A, the angles between planes are 108.37 and 113.39, respectively. Also, The variation in the angles can be obtained due to the volume of the mono-substituted aromatic fragment from the ligands from complex IIa to the ethanol fragment in the ligand of complex A.
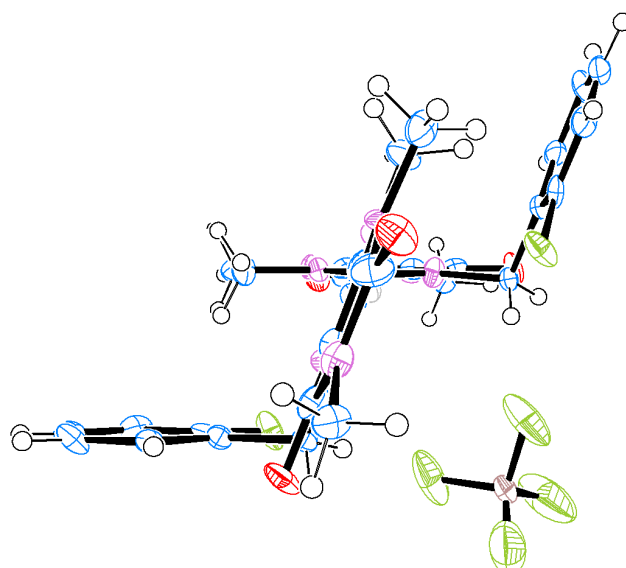
(A) Complex IIa
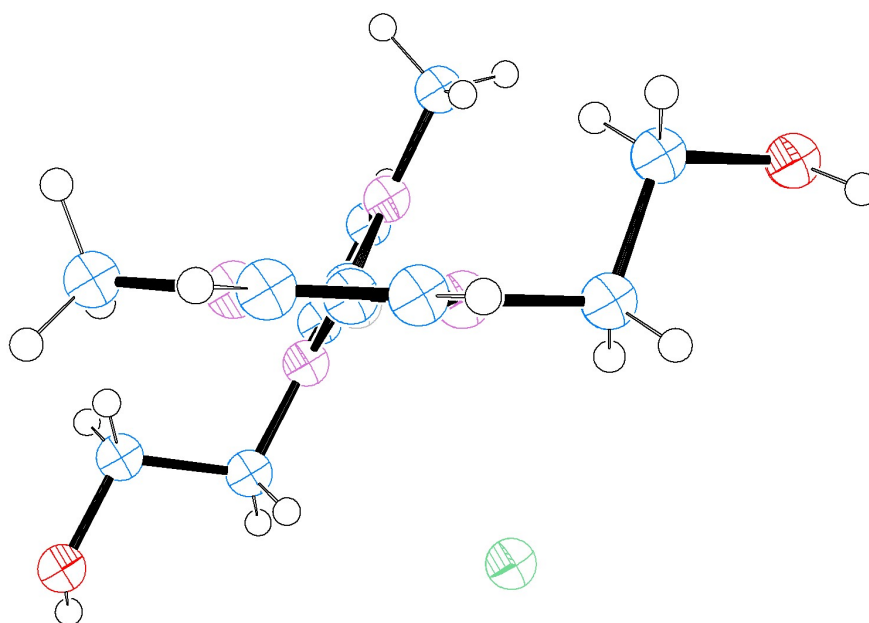
(B) Complex A

FIGURE 3.16: Lateral view for complex IIa and complex A
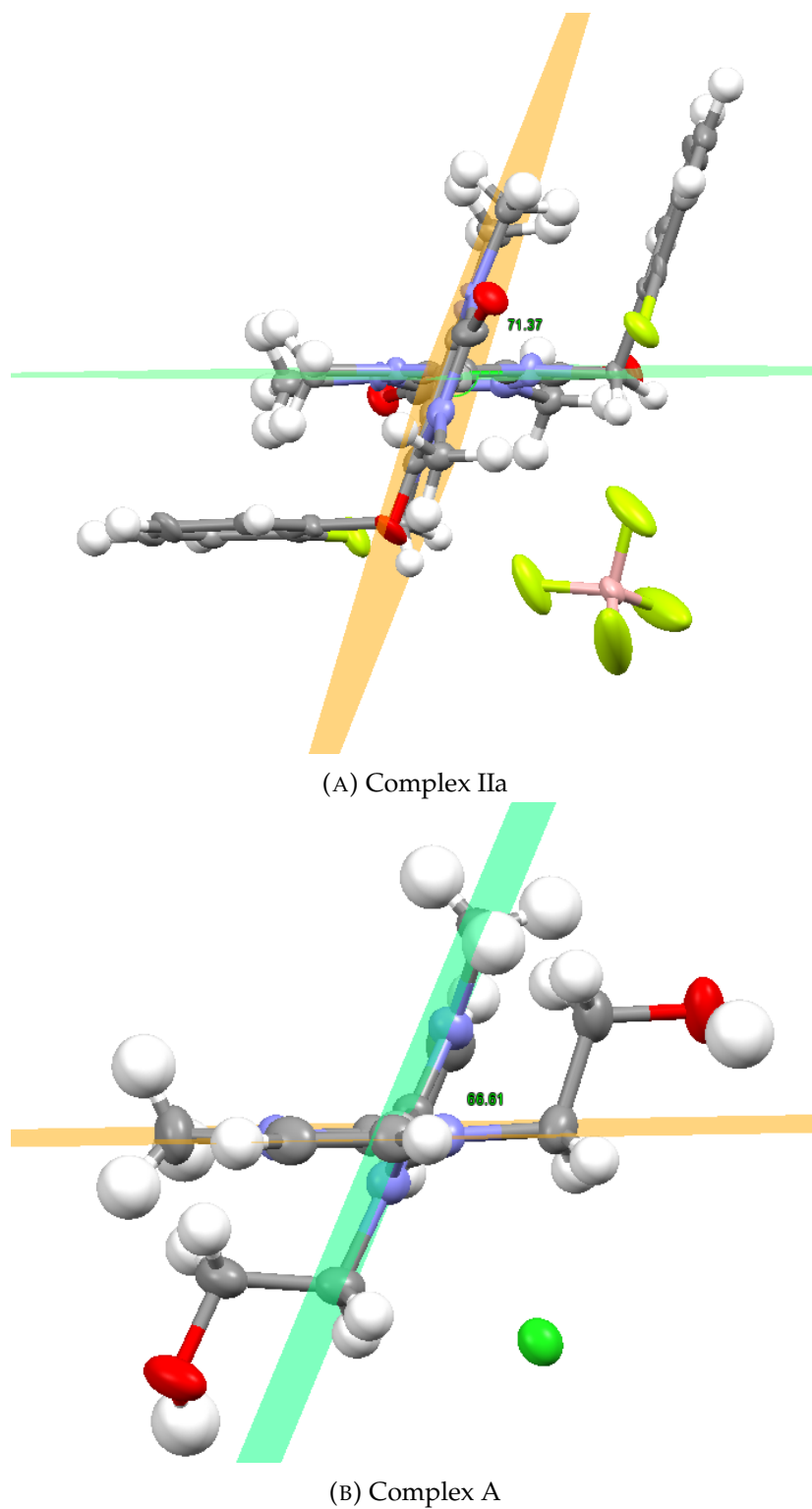
(A) Complex IIa

(B) Complex A

FIGURE 3.17: Angle between planes for complexes IIa and A. A) Planes formed among N(1)-C(2)-N(3) and N(1)*-C(2)*-N(3)* in complex IIa; B) Planes formed among N(1)-Ag(1)-N(2) and N(1)*-Ag(1)*-N(2)* in complex A.

Furthermore, the unit cell of complex IIa (figure 3.20) shows a pattern of stacking among the molecules. There is a $\pi - \pi$ stacking between the six-member ring of the theophylline fragment and the aromatic ring from two molecules, the distance between these rings is 3.386 Å as can be observed in figure 3.19. The molecules do not show hydrogen bonds which can strengthen the intermolecular interactions. The lack of intermolecular interactions makes the complex unstable once the solvent is removed. This directly impacts the few times the compound takes to start the degradation process.
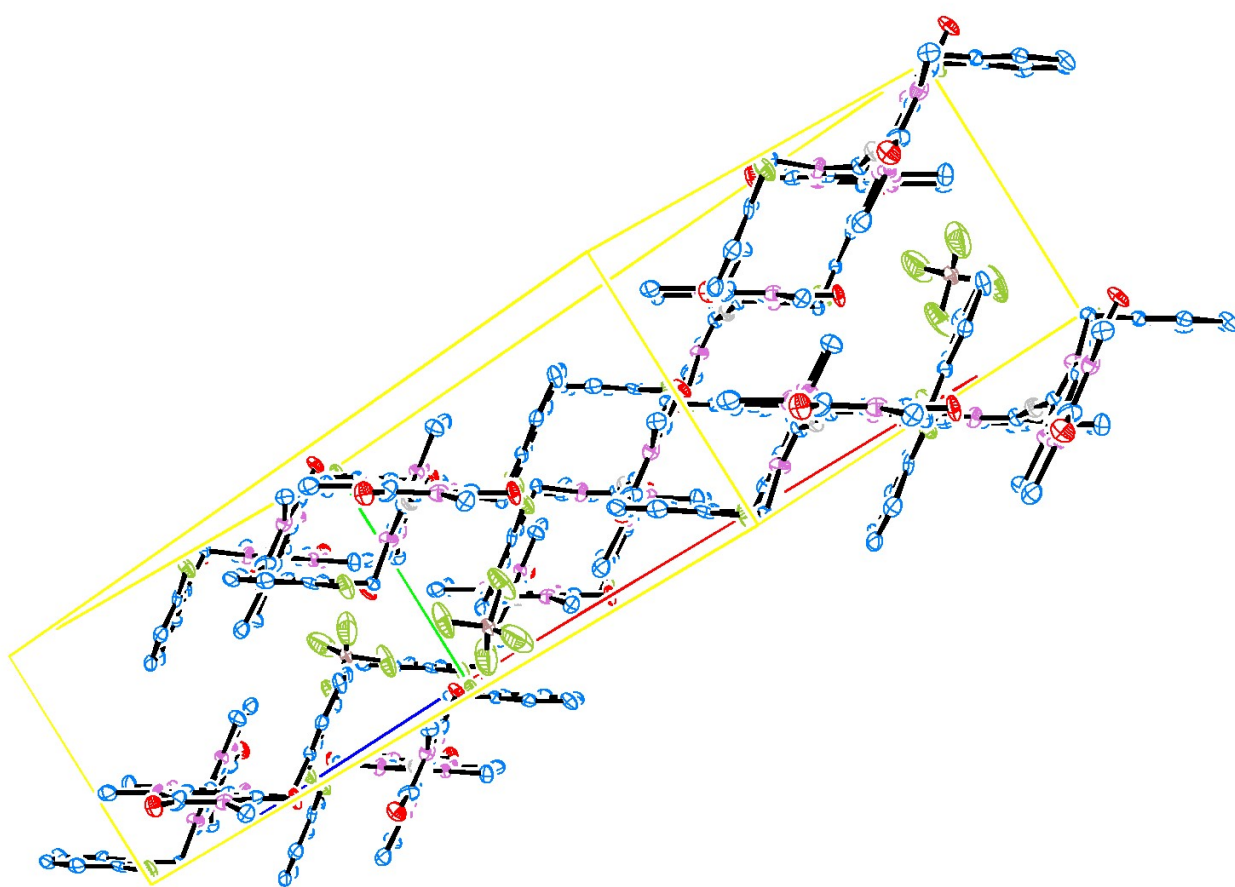

FIGURE 3.18: Unit cell of complex IIa.
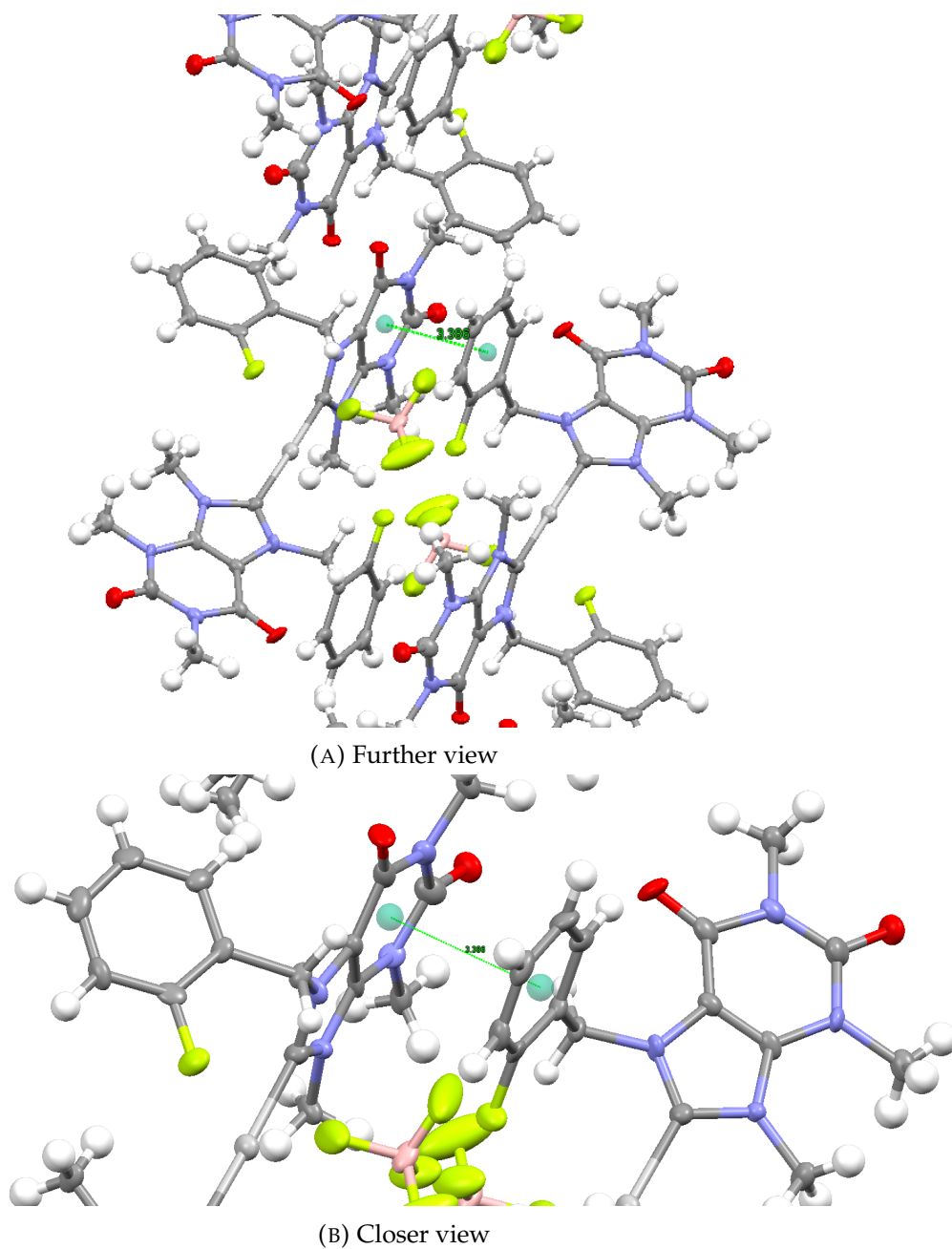
(A) Further view

(B) Closer view

FIGURE 3.19: $\pi - \pi$ stacking distance between the six-member ring of the theophylline fragment and the mono-substituted aromatic ring from different molecules

3.1.5 Cytotoxic activity of the compounds

The preliminary cytotoxic activity of the complexes IIa-e was performed with five human cancer cell lines; human malignant glioblastoma multiforme (U-251), leukemia (K-562), and adenocarcinoma of human prostate (PC-3), breast (MCF-7), lungs (SKLU-1). Also, healthy cells from a green African monkey (COS-7) were included to compare with the cancer cell lines. Furthermore, the complexes were compared with a metallodrug approved by the Food and Drug Administration (FDA), and then, cisplatin was evaluated in the same conditions as the complexes IIa-e. Table 3.5 shows the results obtained at $25\mu M$ of each compound and DMSO as the carrier. However, the results obtained at $25\mu M$ do not provide information regarding the effect of the complexes over the cancer cell lines compared to the health cell line. Therefore, the primary screening was performed at $5\mu M$ (table 3.6)

Compound	HCT-15	U-251	PC-3	K-562	MCF-7	SKLU-1	COS-7
IIa	100	100	100	70.9	83.0	98.9	90.1
IIb	100	100	100	75.7	59.0	100	62.6
IIc	100	100	100	62.5	97.7	100	97.6
IId	100	100	100	67.6	43.23	100	NC
IIe	64.9	48.0	26.2	72.7	15.0	95.2	32.2
cisplatin (10 μM)	36.7	48.4	45.9	36.4	20.3	77.5	42.8

TABLE 3.5: Growth inhibition (%) of cell lines due to the action of the Ag(I) NHC complexes with a 25 μM dosage. (NC=non-cytotoxic)

Compound	HCT-15	U-251	PC-3	K-562	MCF-7	SKLU-1	COS-7
IIa	NC	16.8	NC	38.7	NC	NC	1.3
IIb	2.73	35.2	NC	73.8	2.0	9.1	22.4
IIc	1.38	25.9	NC	100	24.5	10.1	16.7
IId	3.75	22.0	NC	72.0	14.5	7.4	16.5
IIe	1.18	20.2	12.2	57.2	18.6	8.6	14.9
cisplatin (10 μM)	33.6	57.4	57.4	73.2	53.4	89.8	68.6

TABLE 3.6: Growth inhibition (%) of cell lines due to the action of the Ag(I) NHC complexes with a 5 μM dosage. (NC=non-cytotoxic)
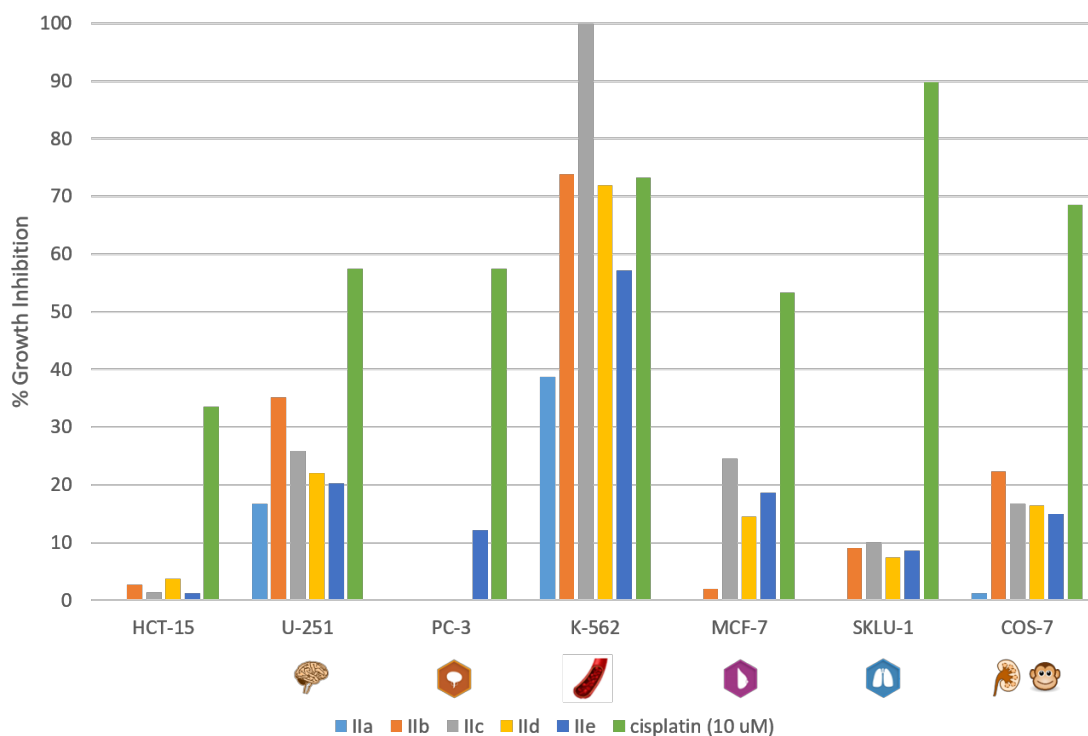
FIGURE 3.20: Growth Inhibition (%) due to the action of Ag (I) complexes at 5 μM with DMSO as carrier

Compound IIa has a good impact on the inhibition for U-251 and K-562 with 16.8 and 38.7%; these values are compared to the healthy cells from the COS-7 line with 1.3% of inhibition. Then, complex IIa can be considered active and selective towards U-251 and K-562. It does not present activity (non-cytotoxic) over PC-3, MCF-7, and SKLU-1.

Complexes IIb-c are selective and active over the K-562 cell line with 73.8% and 100% growth inhibition, respectively; they are non-cytotoxic over PC-3; and in the rest of the cell lines, the effect is less than the one in the COS-7 cell line.

Complexes IId-e present activity and selectivity in the K-562 cell line with 72.0% and 57.2% growth inhibition, respectively.

3.2 Conclusions and future work

It has been synthesized and characterized a series of five nobel Ag(I) NHC complexes derived from theophylline. The molecular structure of complex IIa was determined unequivocally through single-crystal X-ray diffraction; within the figures, we can appreciate the NHC ligands coordinated to the Ag(I) atom and a linear geometry. Also, the study of non-covalent interactions in the crystal lattice showed that there was no presence of hydrogen atoms. Furthermore, there is $\pi - \pi$ stacking between the aromatic ring and the antiaromatic ring from different molecules, responsible for the compounds' little stability once the solvent is removed.

Moreover, the *in vivo* cytotoxic assays show no direct relation between the degree of fluorination of the complexes and their activity over the human cancer cell lines. In the inhibition percentage of the health cell lines, the lowest and the highest values are obtained with complexes IIa-b.

Compound IIa exhibits significant inhibitory effects on U-251 and K-562 cell lines, with 16.8% and 38.7% inhibition rates, respectively, compared to the healthy COS-7 cell line, which only showed a 1.3% inhibition rate. Therefore, it can be concluded that compound IIa is both active and selective towards U-251 and K-562 cells, and it does not exhibit cytotoxicity towards PC-3, MCF-7, and SKLU-1 cell lines.

Complexes IIb and IIc exhibit selectivity and activity against the K-562 cell line, resulting in 73.8% and 100% growth inhibition rates, respectively. When tested on the PC-3 cell line, these complexes are non-cytotoxic, and their effects on other cell lines are less pronounced than those observed in the COS-7 cell line.

Complexes IId and IIe also demonstrate activity and selectivity against the K-562 cell line, with 72.0% and 57.2% growth inhibition rates, respectively.

Appendix A
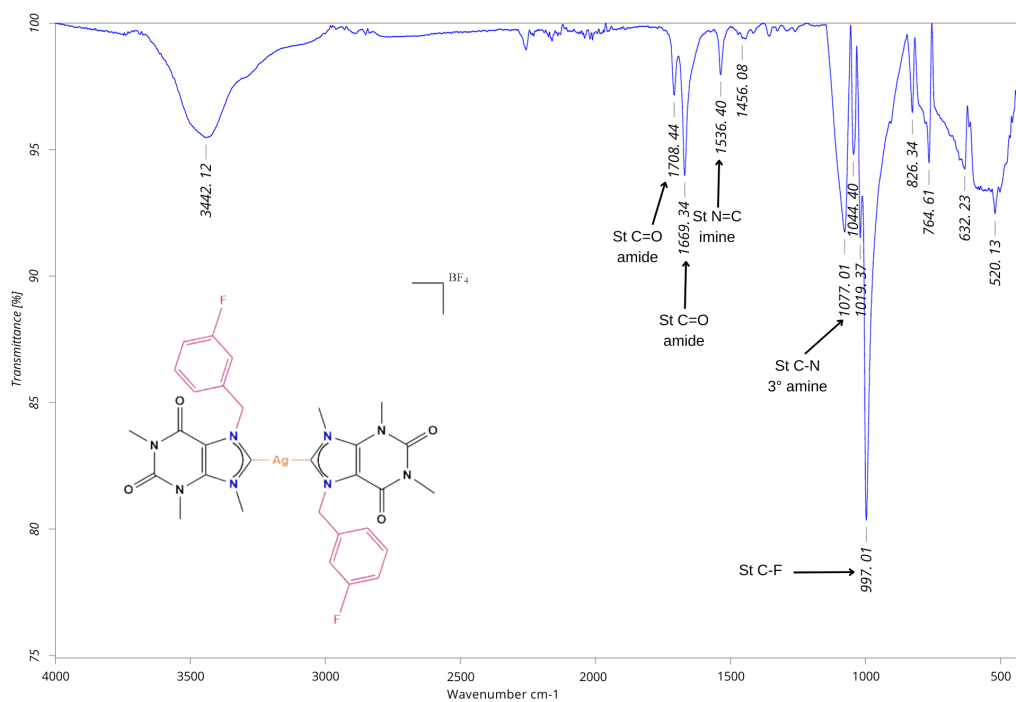
Data analysis

A.1 Complexes FT-IR spectra

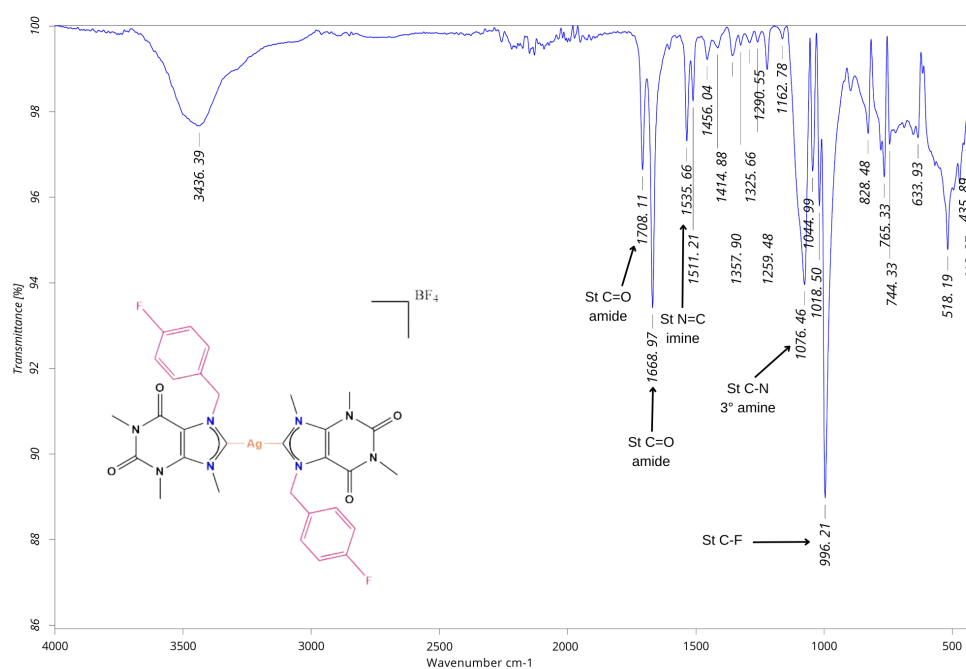FIGURE A.1: FT-IR spectrum of complex IIb, showing the most important stretching bands for the molecule

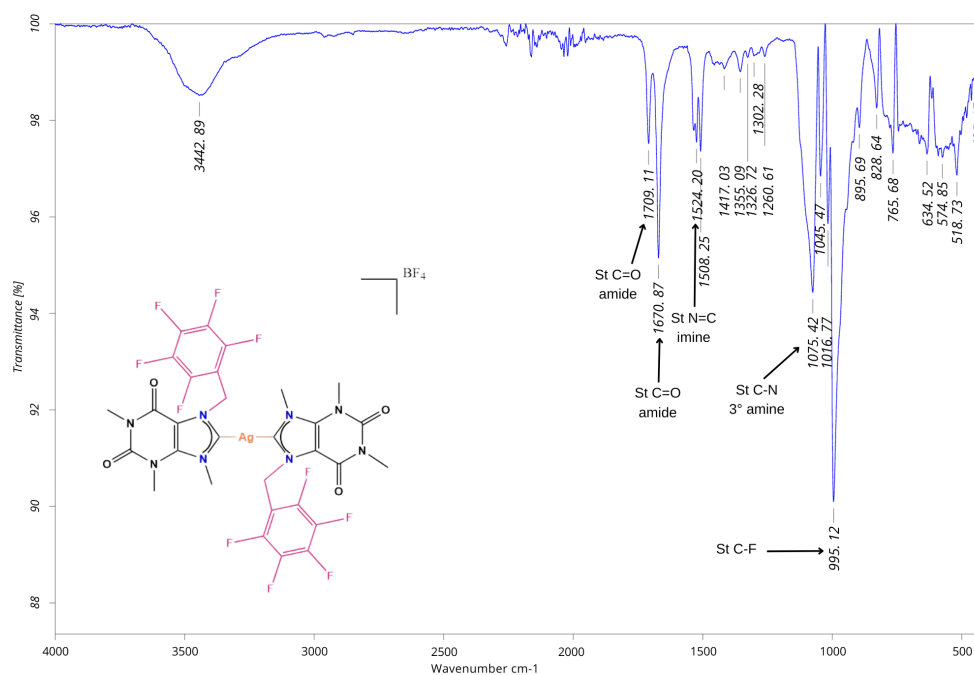FIGURE A.2: FT-IR spectrum of complex IIc, showing the most important stretching bands for the molecule

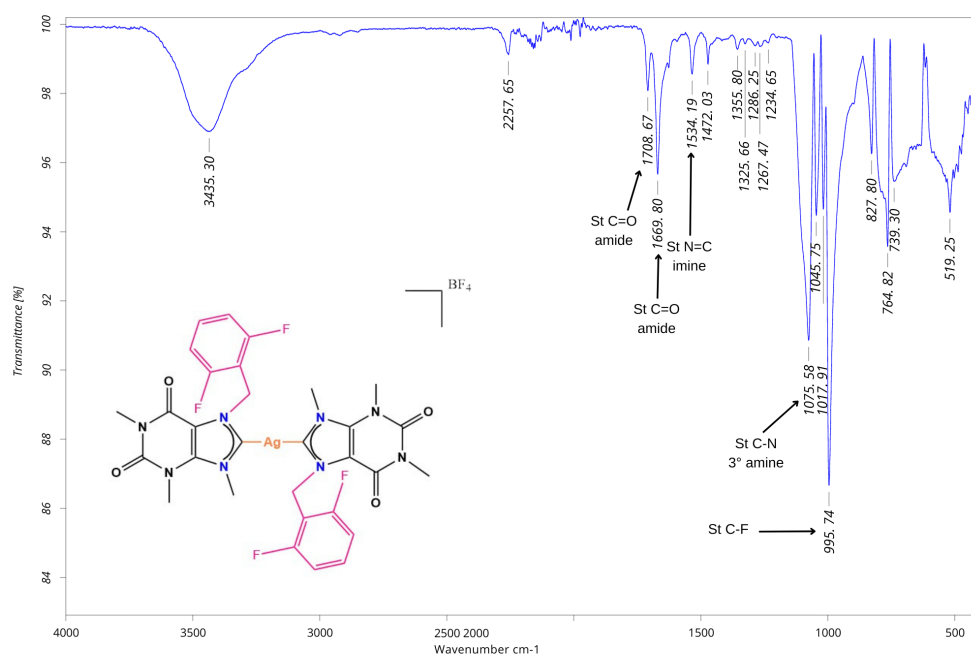FIGURE A.3: FT-IR spectrum of complex IId, showing the most important stretching bands for the molecule

FIGURE A.4: FT-IR spectrum of complex IIe, showing the most important stretching bands for the molecule

A.2 Complexes $^1H - NMR$ and analysis

Peak	Experimental value (ppm)	Theoretical value (ppm)	Integral	Multiplicity	Number of H around
1	3.19	2.2-2.9	6	singlet	0
2	3.77	2.2-2.9	6	singlet	0
3	4.13	3.77-4.27	6	singlet	0
4	5.67	5.68-5.85	4	singlet	0
5	6.76	6.5-8.0	2	doublet	1
6	7.23	6.5-8.0	4	multiplet	2
7	7.26	6.5-8.0	2	multiplet	1
8	7.65	6.5-8.0	2	doublet	2

TABLE A.1: Analysis of the peaks for $^1H\ NMR$ spectrum of compound IIb
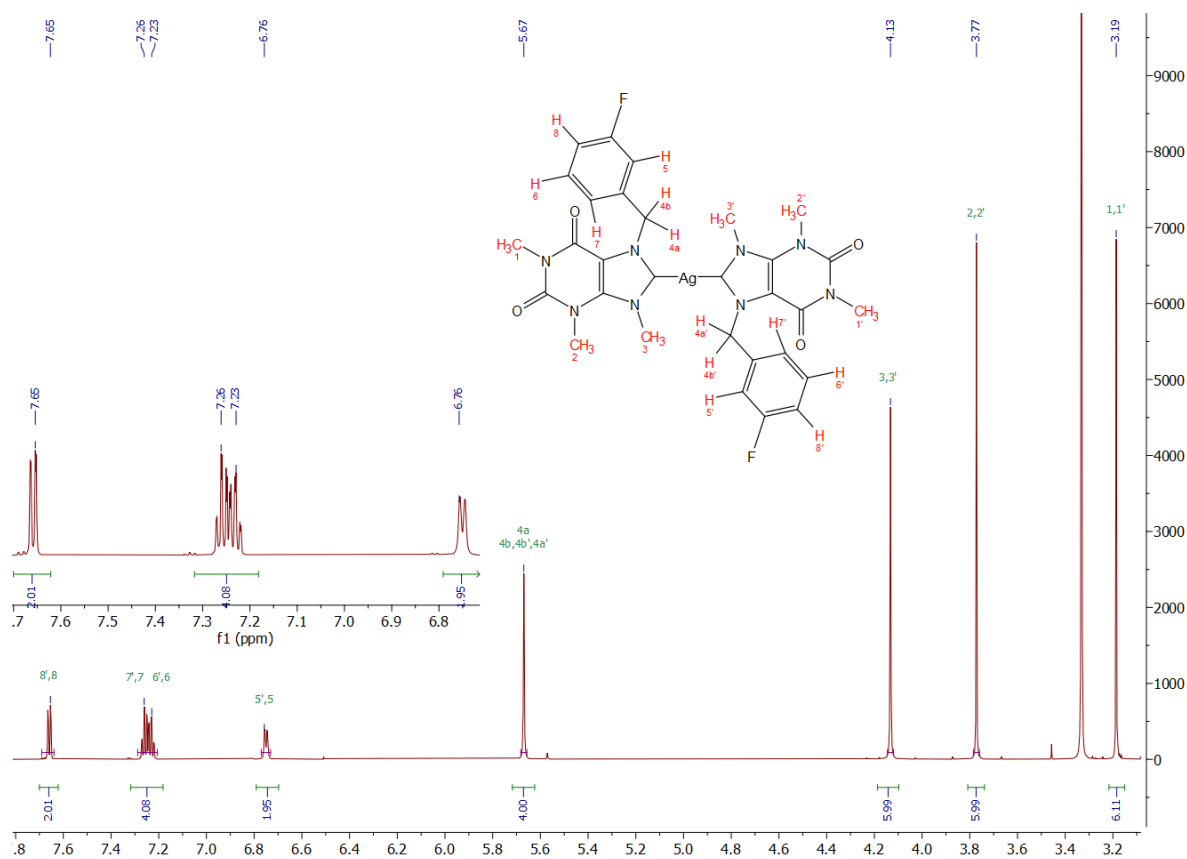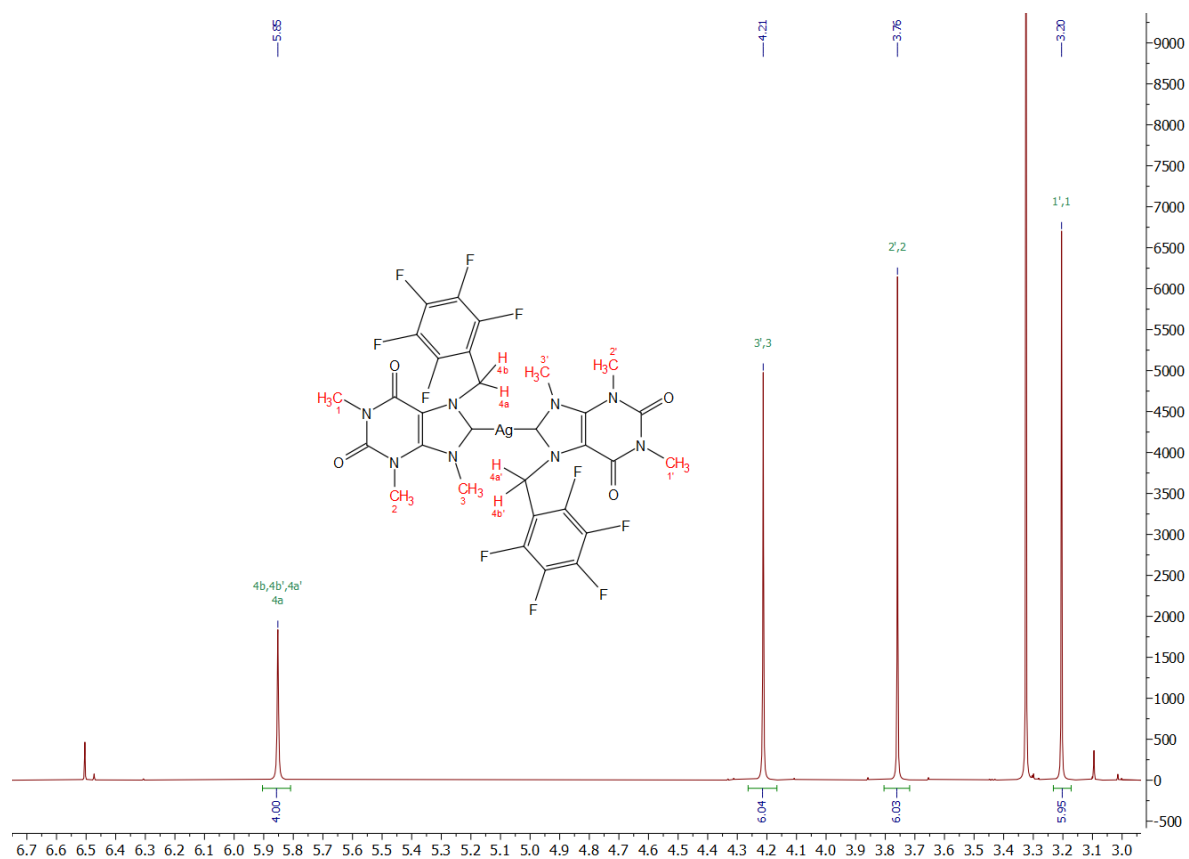
FIGURE A.5: ^1H NMR spectrum (700 MHz, $DMSO - d_6$) of the compound IIb.

Peak	Experimental value (ppm)	Theoretical value (ppm)	Integral	Multiplicity	Number of H around
1	3.23	2.2-2.9	6	singlet	0
2	3.75	2.2-2.9	6	singlet	0
3	4.17	3.77-4.27	6	singlet	0
4	5.65	5.68-5.85	4	singlet	0
5	7.14	6.5-8.0	4	triplet	2
6	7.36	6.5-8.0	4	triplet	2

TABLE A.2: Analysis of the peaks for ^1H NMR spectrum of compound IIc.
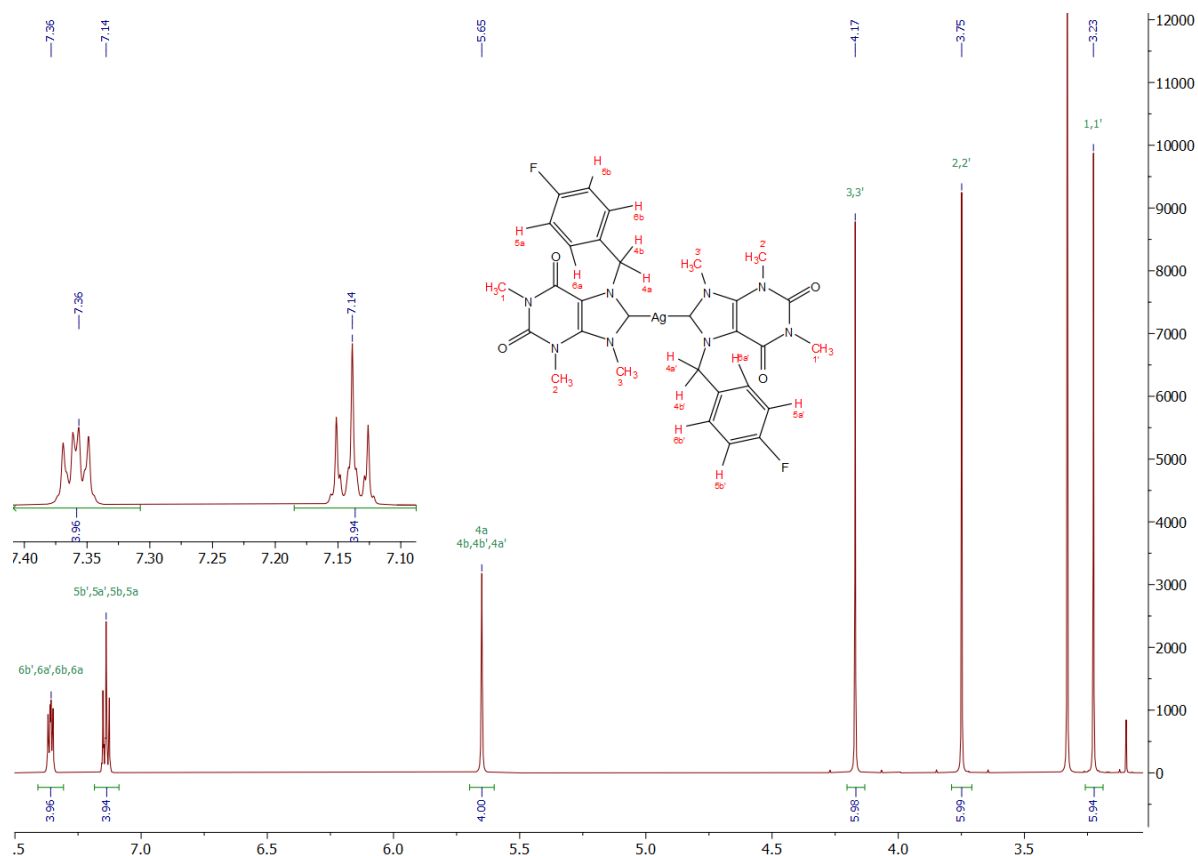
FIGURE A.6: ^1H NMR spectrum (700 MHz, $DMSO - d_6$) of the compound IIc.

Peak	Experimental value (ppm)	Theoretical value (ppm)	Integral	Multiplicity	Number of H around
1	3.20	2.2-2.9	6	singlet	0
2	3.76	2.2-2.9	6	singlet	0
3	4.21	3.77-4.27	6	singlet	0
4	5.85	5.68-5.85	4	singlet	0

TABLE A.3: Analysis of the peaks for ^1H NMR spectrum of compound IId.

FIGURE A.7: ^1H NMR spectrum (700 MHz, $DMSO - d_6$) of the compound IId.

Peak	Experimental value (ppm)	Theoretical value (ppm)	Integral	Multiplicity	Number of H around
1	3.24	2.2-2.9	6	singlet	0
2	3.76	2.2-2.9	6	singlet	0
3	4.08	3.77-4.27	6	singlet	0
4	5.73	5.68-5.85	4	singlet	0
5	7.09	6.5-8.0	4	multiplet	1
6	7.42	6.5-8.0	4	multiplet	2

TABLE A.4: Analysis of the peaks for ^1H NMR spectrum of compound IIe.
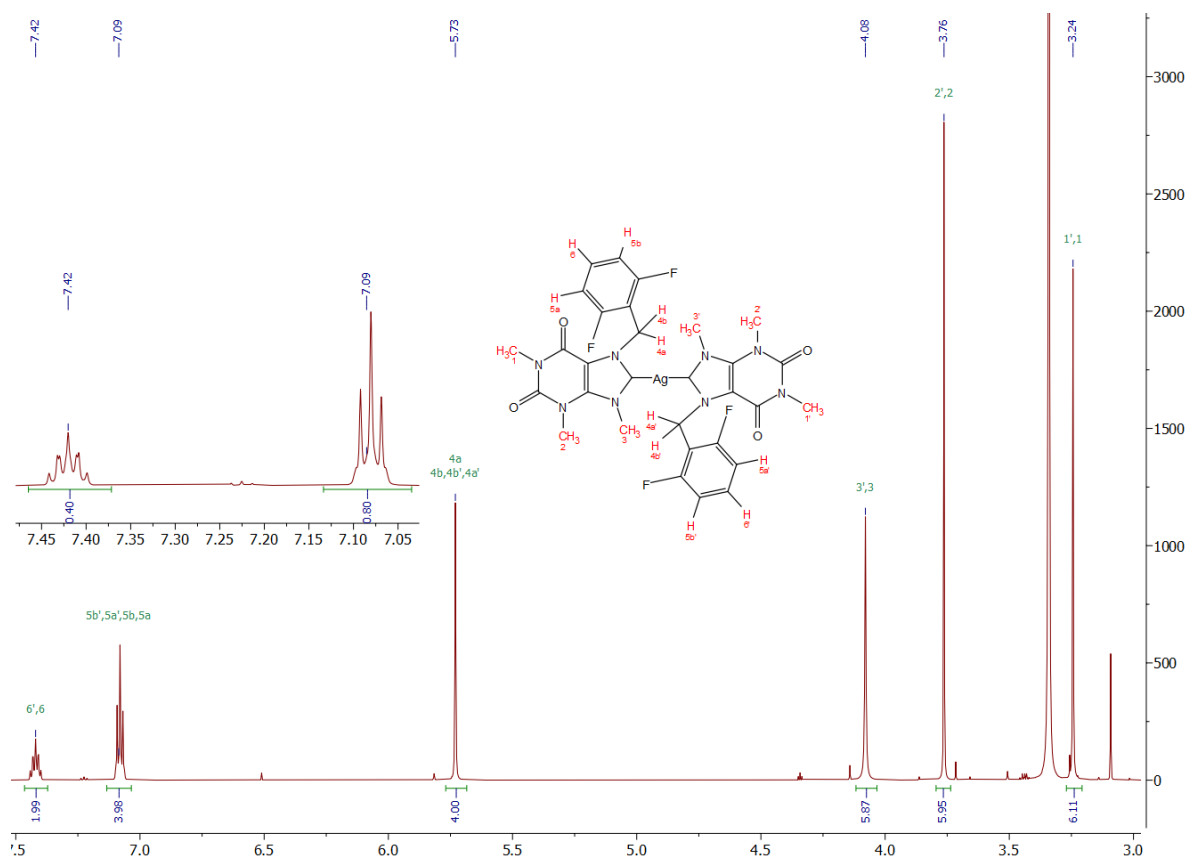
FIGURE A.8: ^1H NMR spectrum (700 MHz, $DMSO - d_6$) of the compound IIe.

A.3 *FAB$^+$* **mass spectra for complexes IIb-c**
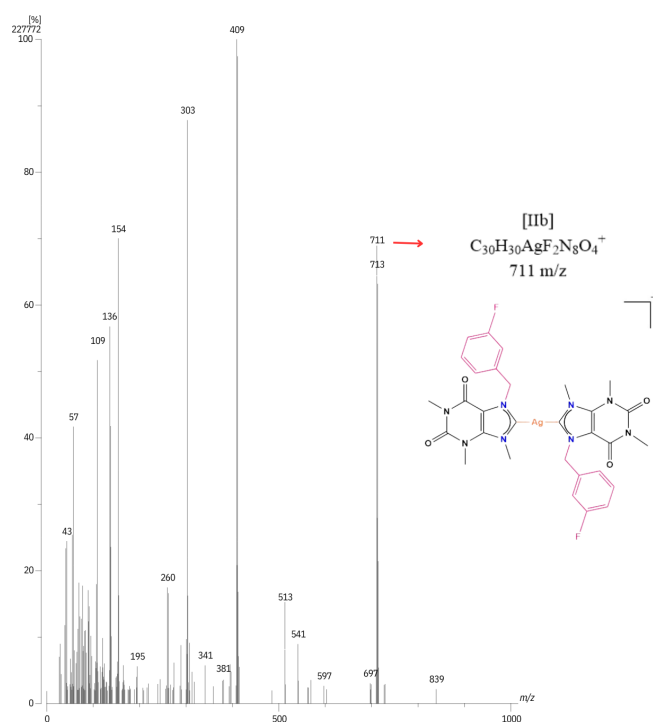
FIGURE A.9: *FAB$^+$* mass spectrum of the IIb complex
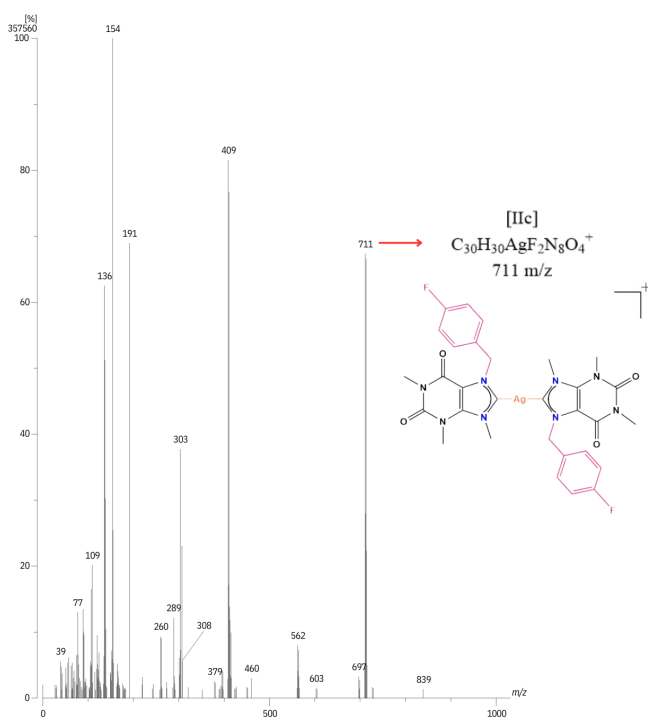
FIGURE A.10: *FAB$^+$* mass spectrum of the IIc complex

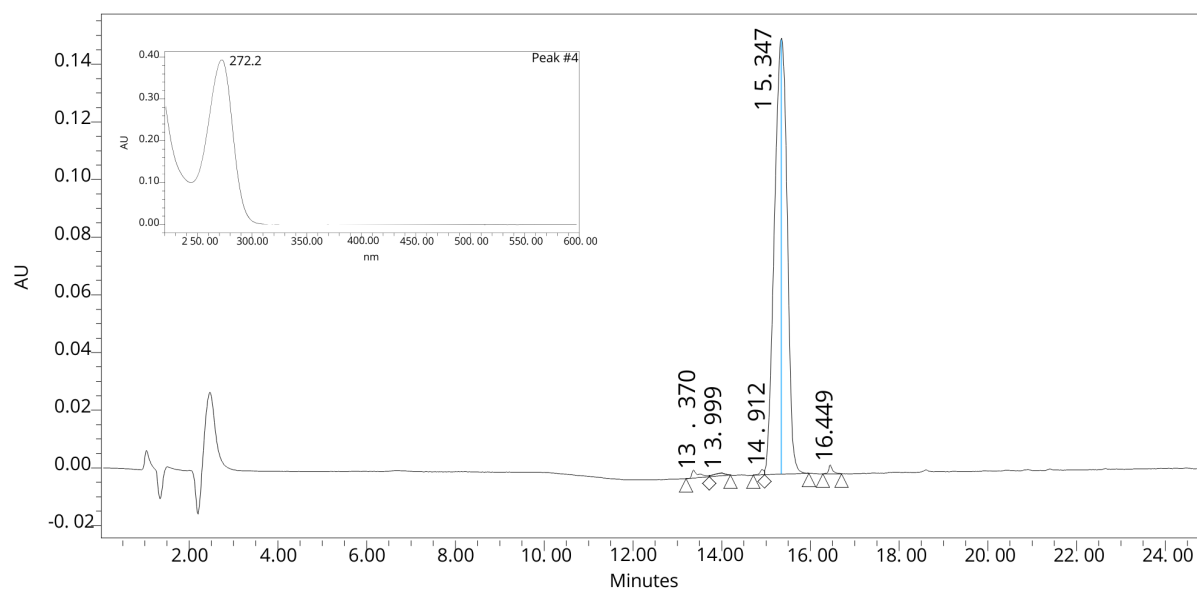# A.4 HPLC chromatograms of complexes IIa-e
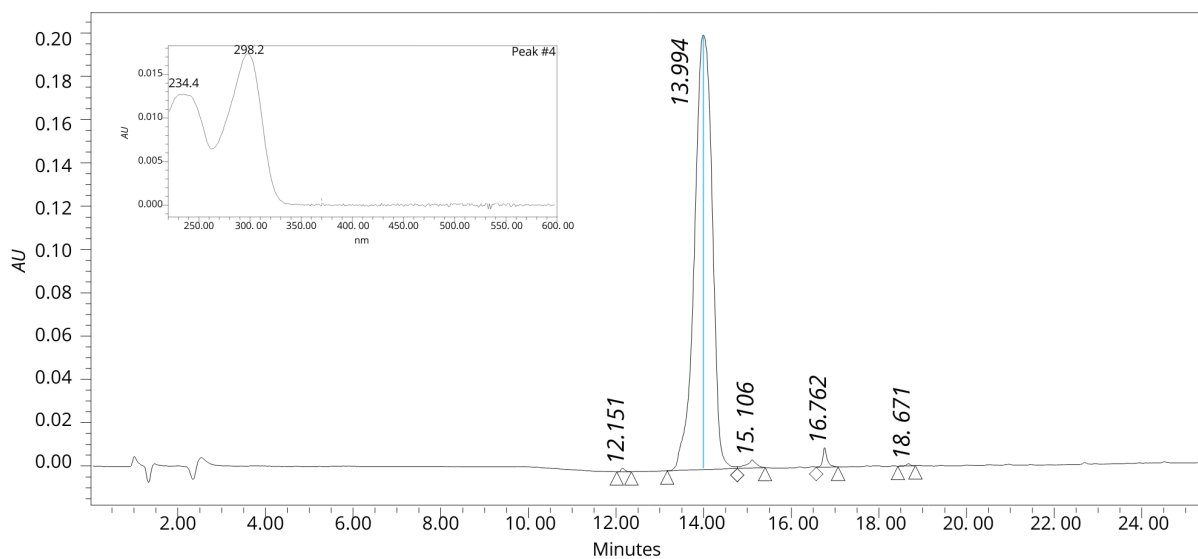
FIGURE A.11: HPLC chromatogram of IIb complex. RP-HPLC: [linear gradient ACN/H_2O (5:95) to (100:0) over 20 min].
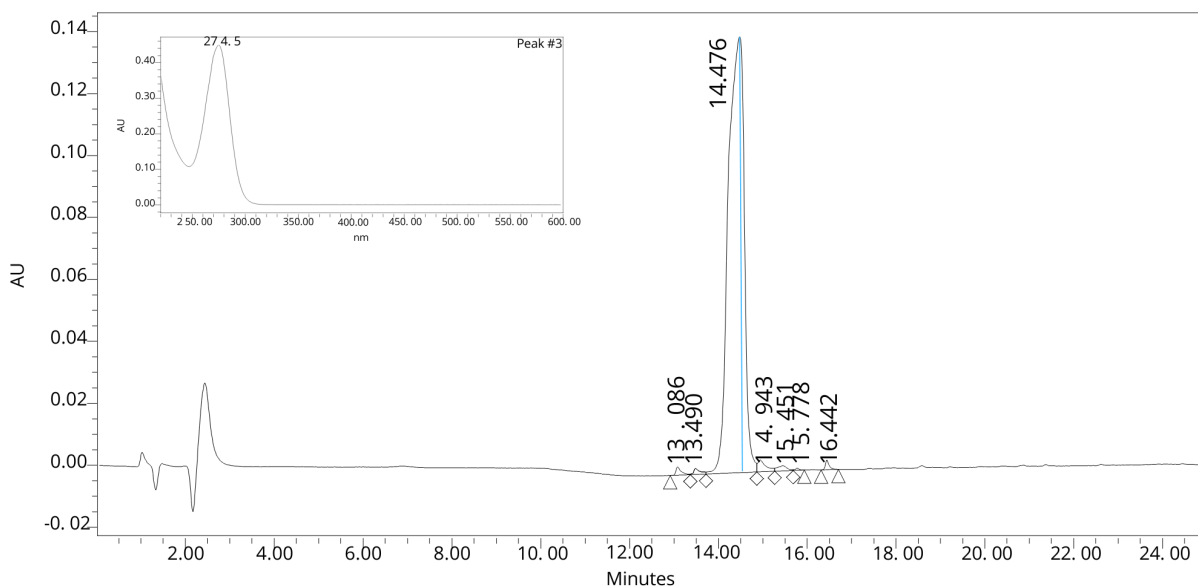

FIGURE A.12: HPLC chromatogram of IIc complex. RP-HPLC: [linear gradient ACN/H_2O (5:95) to (100:0) over 20 min].

FIGURE A.13: HPLC chromatogram of IId complex. RP-HPLC: [linear gradient ACN/H_2O (5:95) to (100:0) over 20 min].
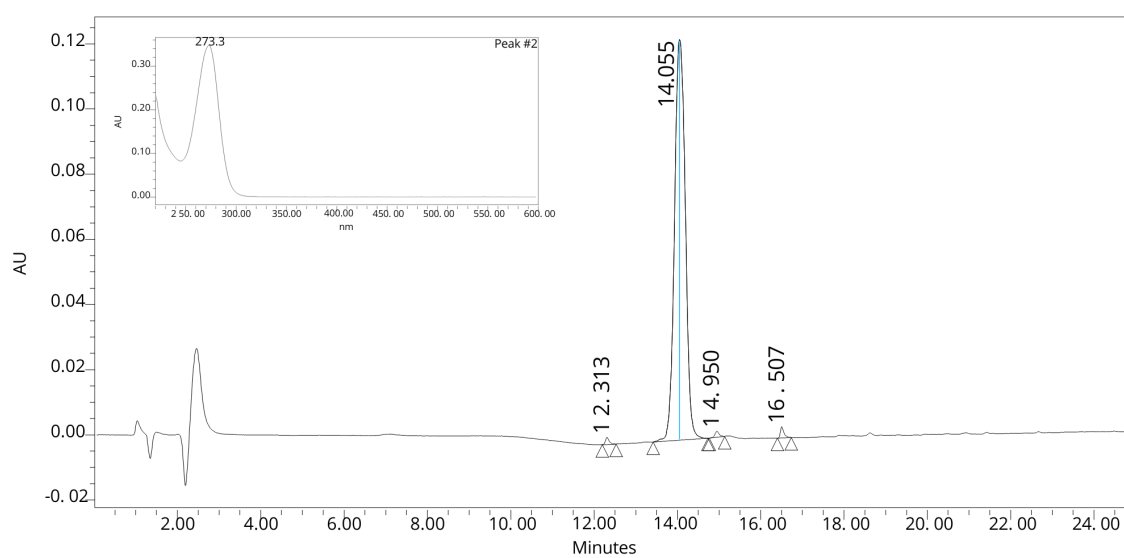
FIGURE A.14: HPLC chromatogram of IIe complex. RP-HPLC: [linear gradient ACN/H_2O (5:95) to (100:0) over 20 min].

A.5 $^{13}C\{^1H\}$ NMR spectra assignation
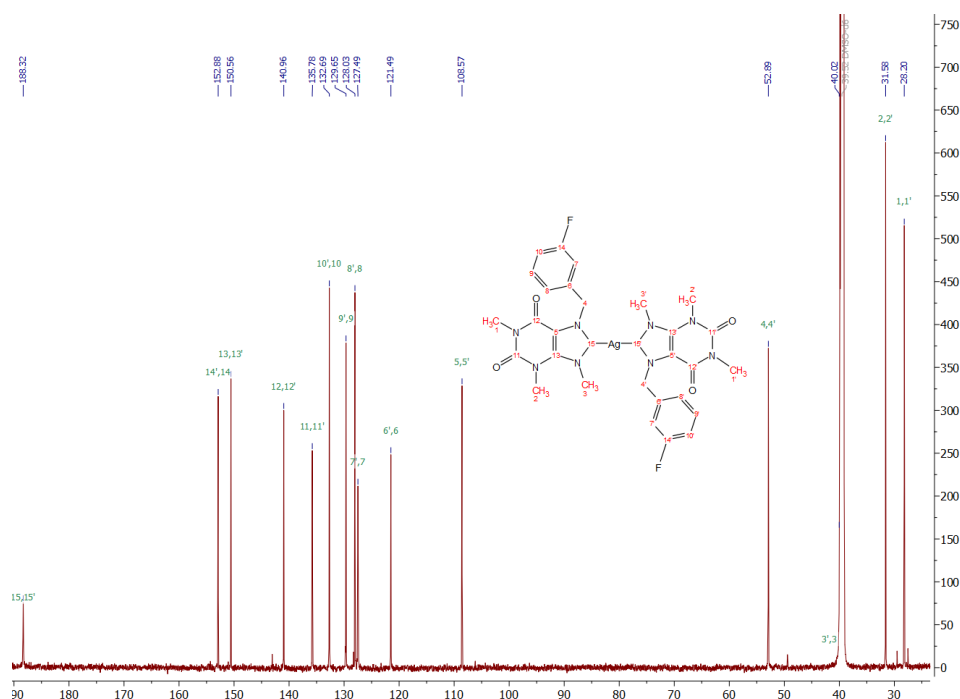
FIGURE A.15: $^{13}C\{^1H\}$ NMR spectrum (176 MHz, $DMSO - d_6$) of compound IIb.
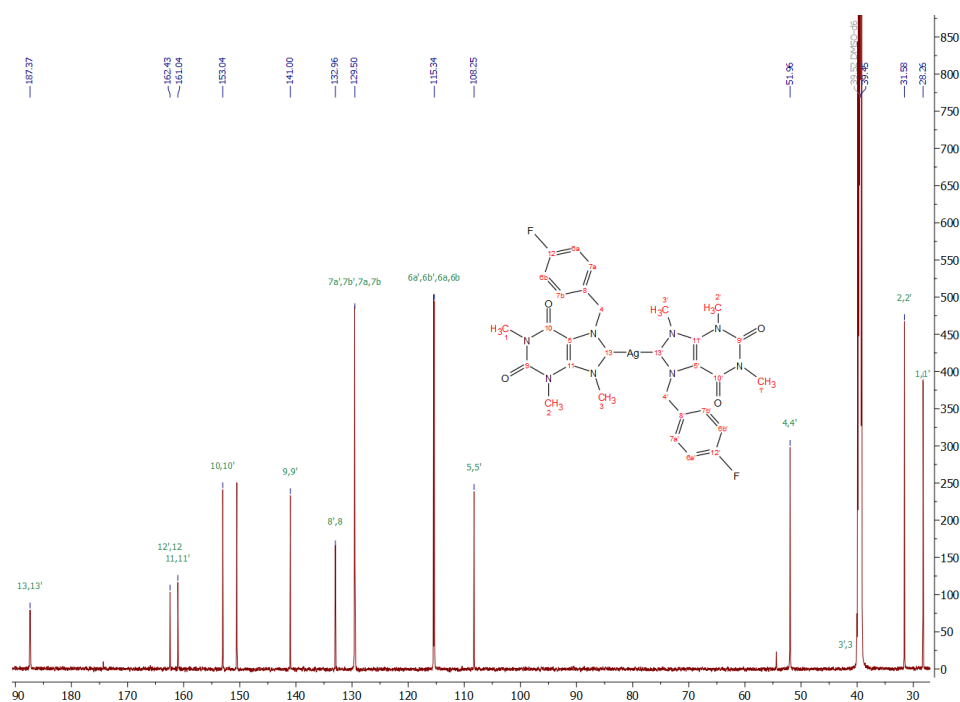
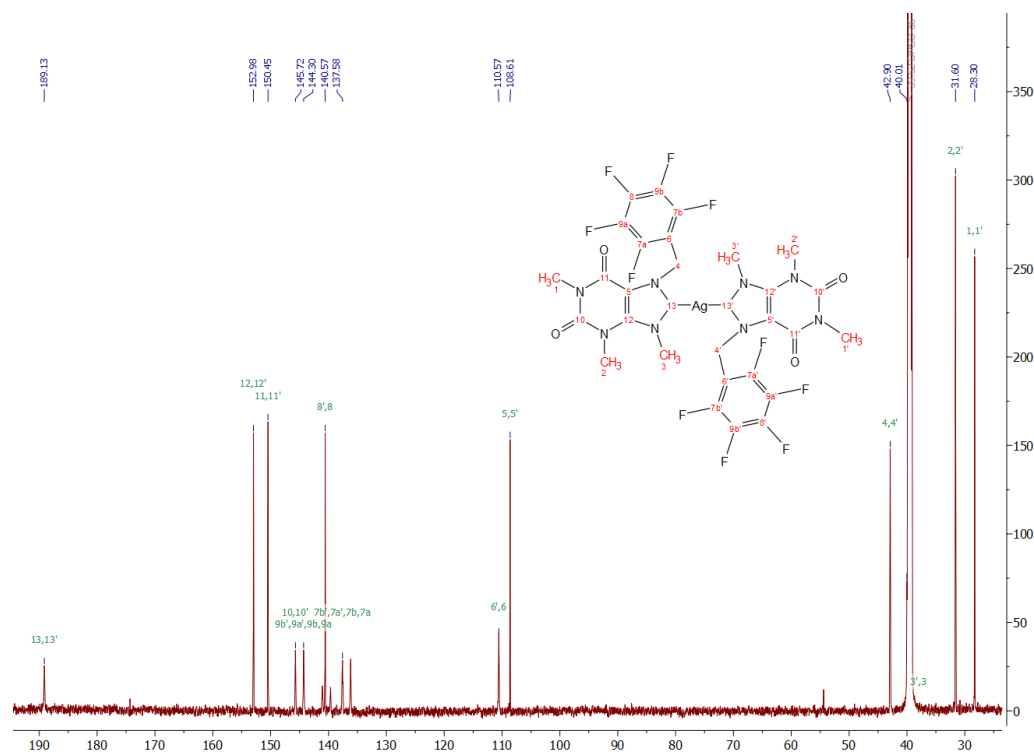FIGURE A.16: $^{13}C\{^1H\}$ NMR spectrum (176 MHz, $DMSO - d_6$) of compound IIc.

FIGURE A.17: $^{13}C\{^1H\}$ NMR spectrum (176 MHz, $DMSO - d_6$) of compound IId.

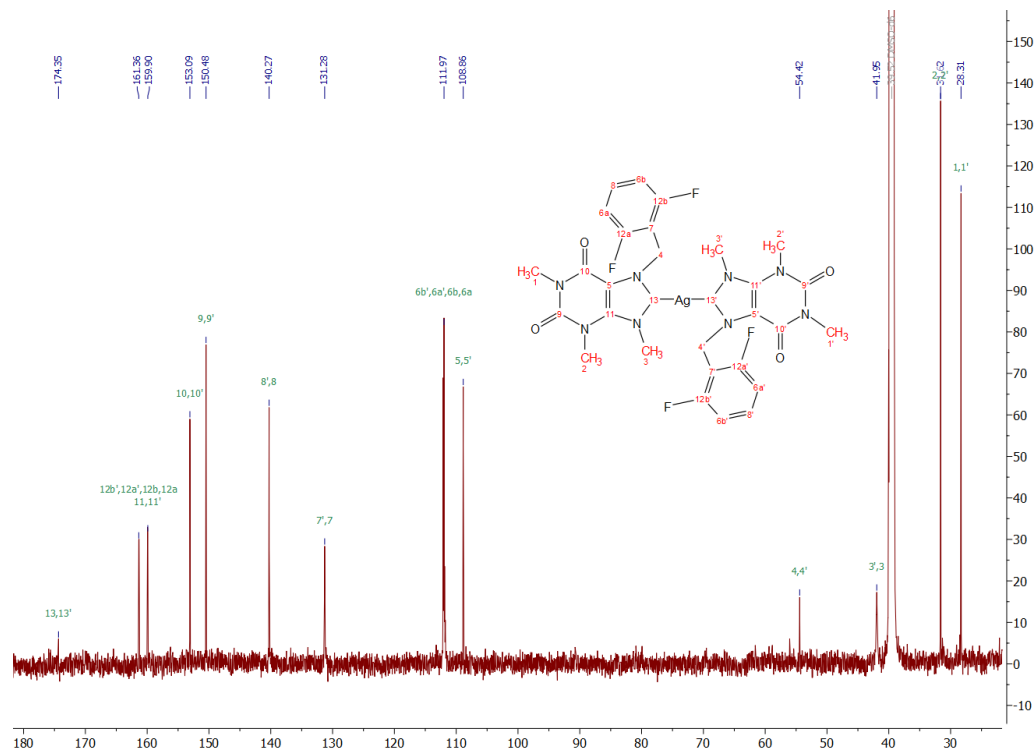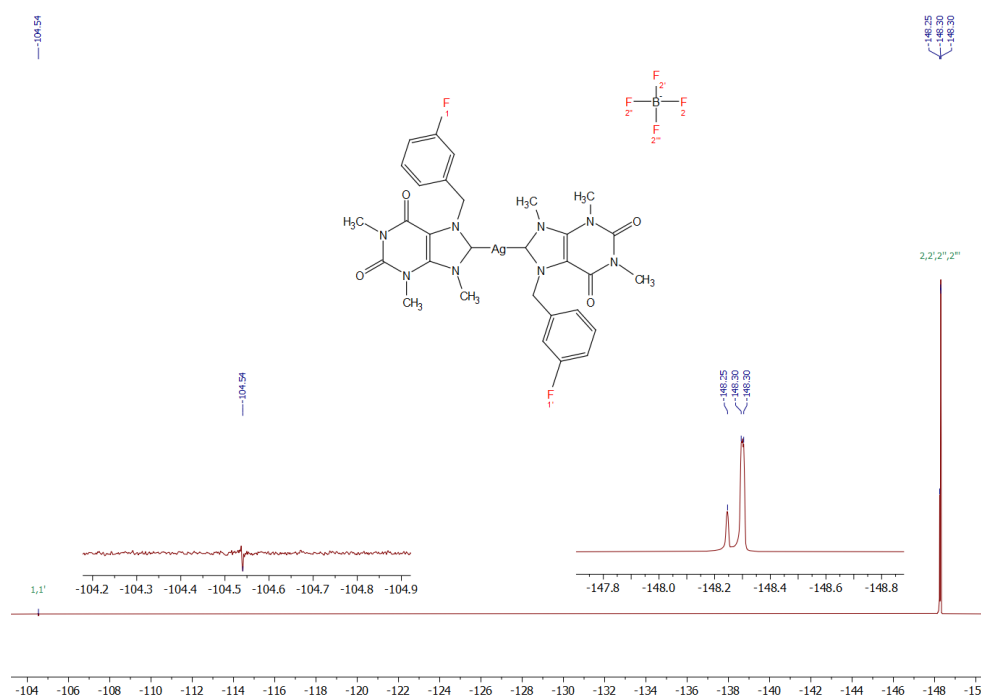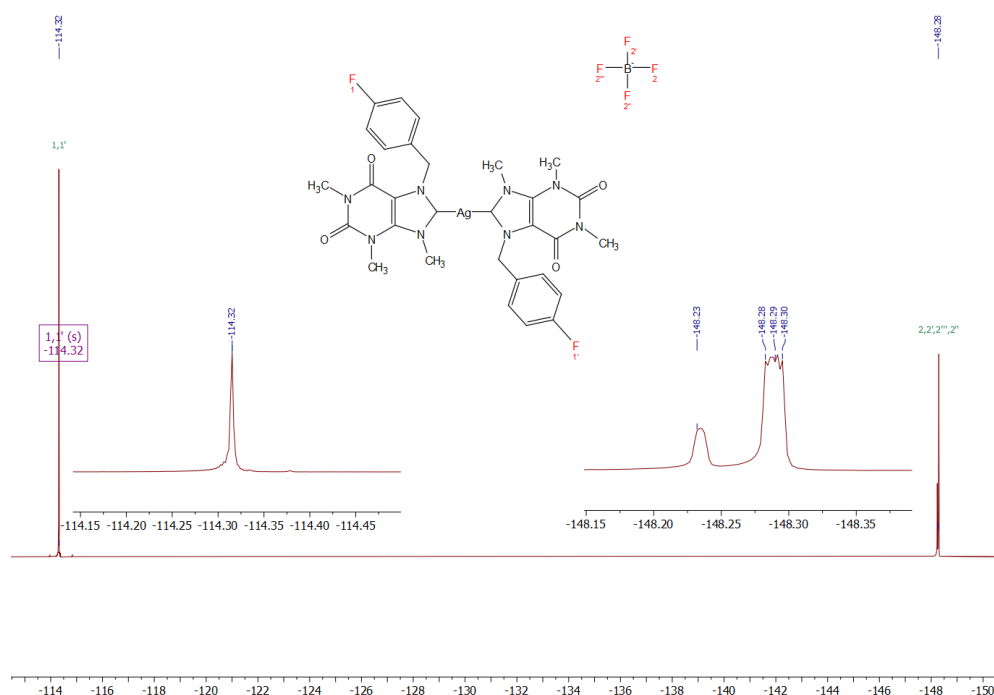FIGURE A.18: $^{13}C\{^1H\}$ NMR spectrum (176 MHz, $DMSO - d_6$) of compound IIe.

A.6 ^{19}F NMR spectra assignation

FIGURE A.19: ^{19}F NMR spectrum (282 MHz, $DMSO - d_6$) of compound IIb.

FIGURE A.20: ^{19}F NMR spectrum (282 MHz, $DMSO - d_6$) of compound IIc.
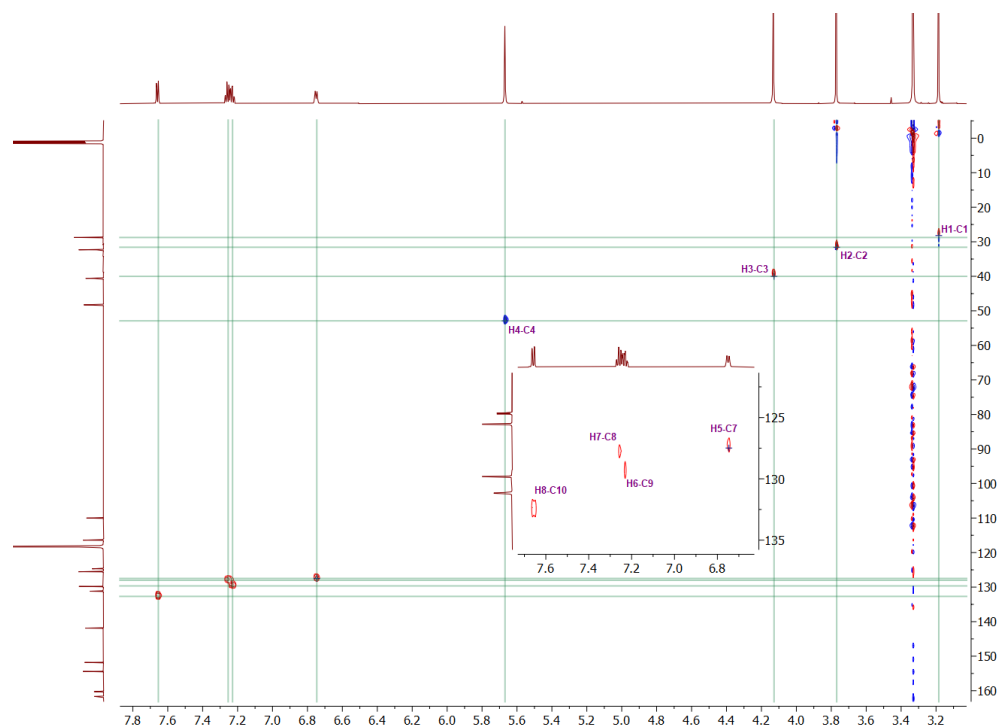
A.7 Heteronuclear Single Quantum Coherence (HSQC)

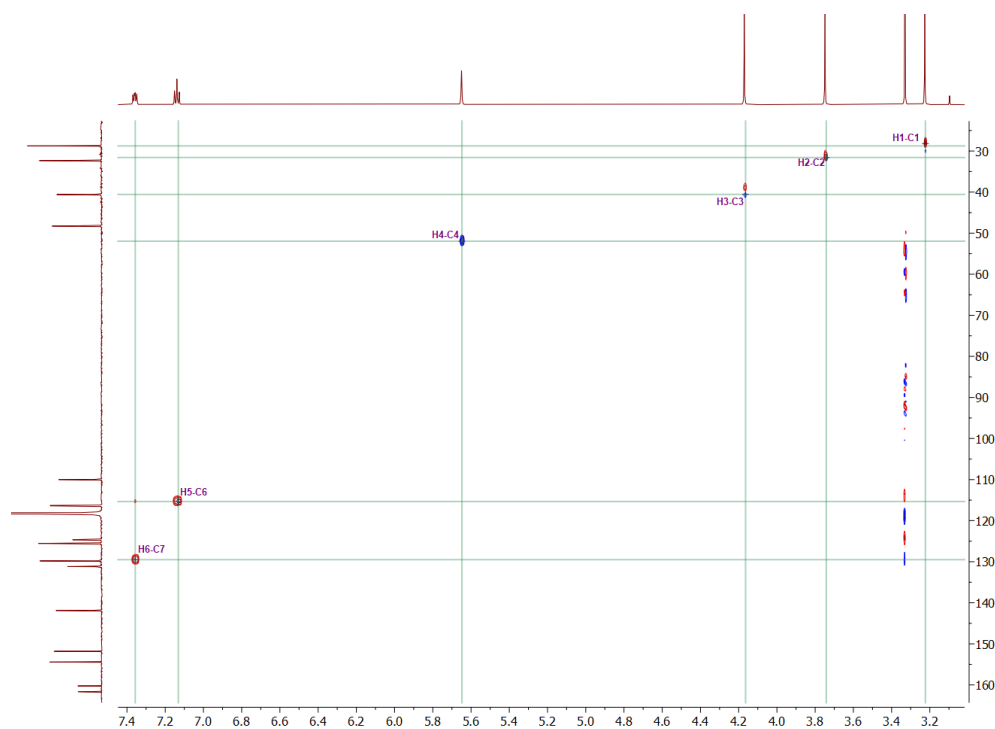FIGURE A.21: HSQC spectrum ($^1H = 700\ MHz\ and\ ^{13}C = 176\ MHz$, $DMSO - d_6$) of compound IIb.

FIGURE A.22: HSQC spectrum ($^1H = 700\ MHz\ and\ ^{13}C = 176\ MHz$, $DMSO - d_6$) of compound IIc.
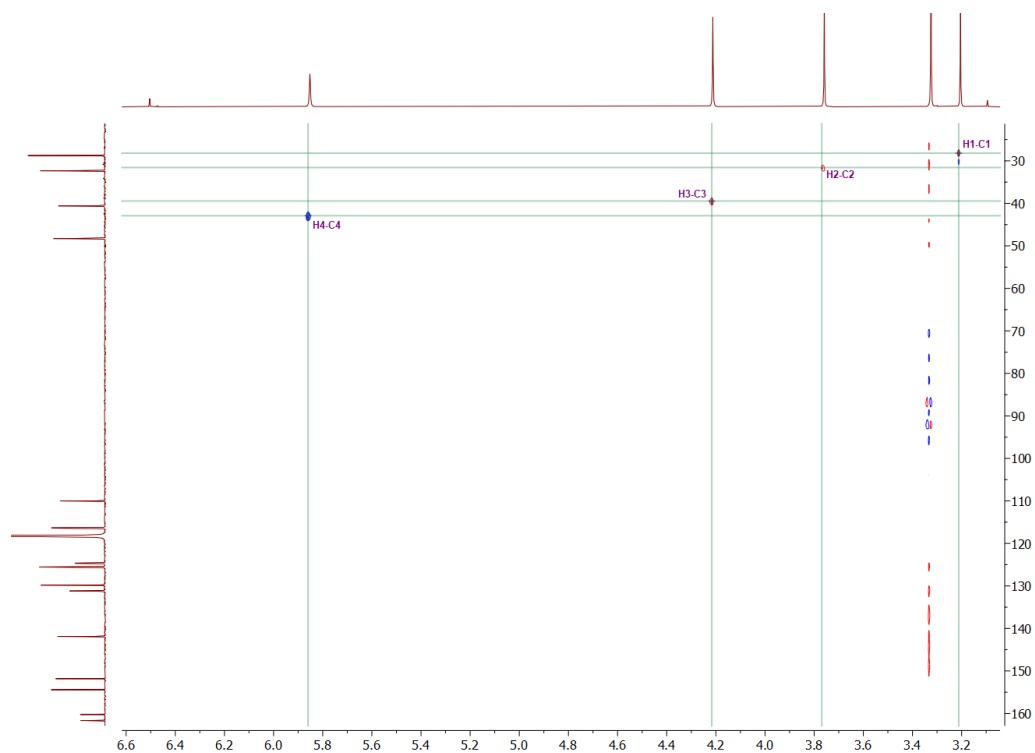
FIGURE A.23: HSQC spectrum ($^1H = 700\ MHz$ and $^{13}C = 176\ MHz$, $DMSO - d_6$) of compound IId.
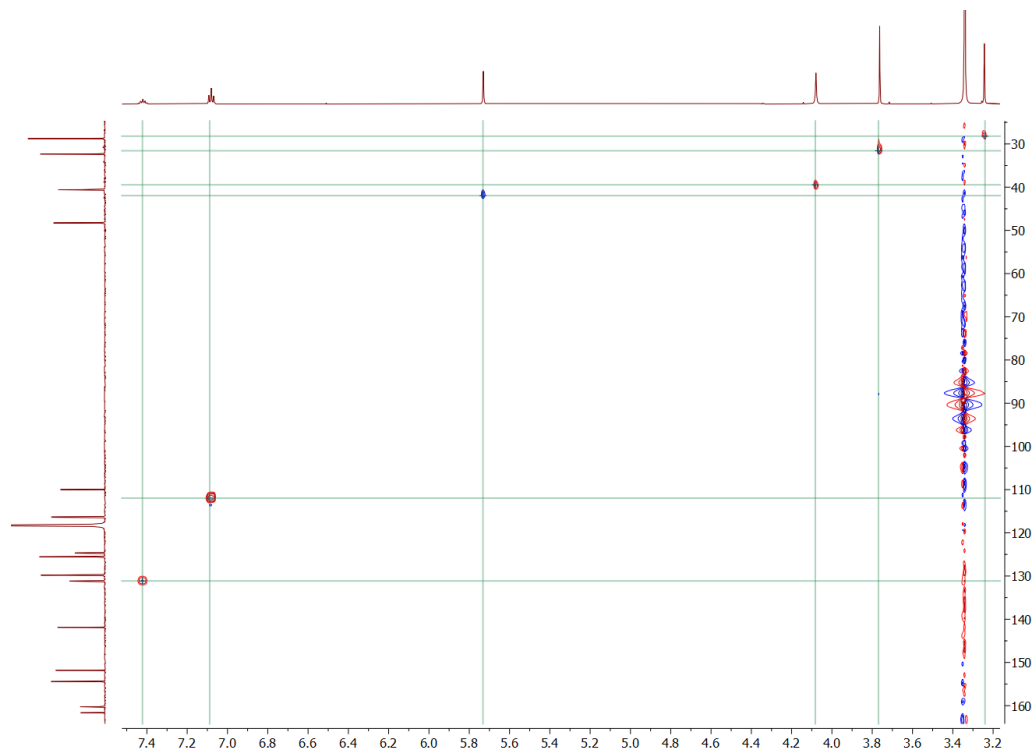

FIGURE A.24: HSQC spectrum ($^1H = 700\ MHz$ and $^{13}C = 176\ MHz$, $DMSO - d_6$) of compound IIe.

A.8 Heteronuclear Multiple Bond Correlation (HMBC)

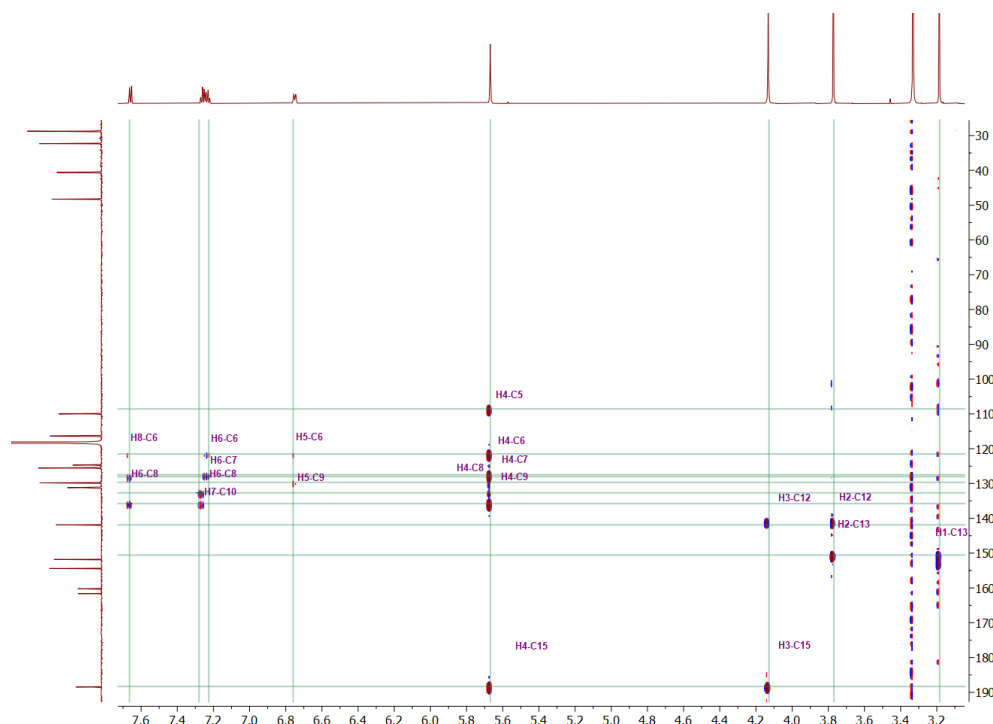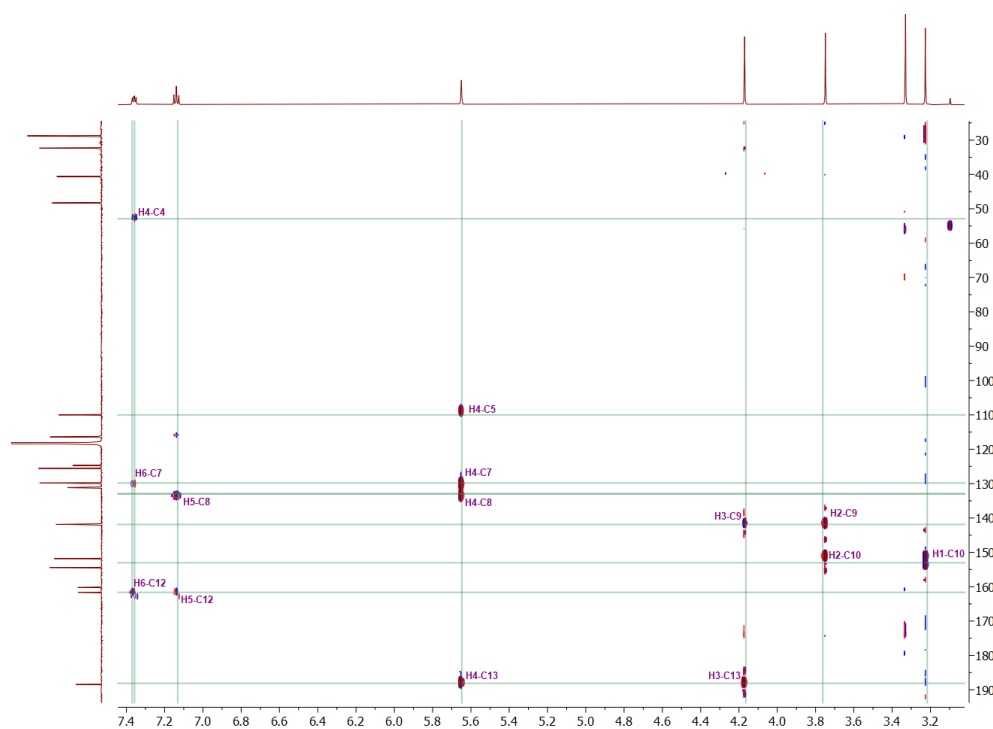FIGURE A.25: HMBC spectrum ($^1H = 700\ MHz\ and\ ^{13}C = 176\ MHz$, $DMSO - d_6$) of compound IIb.

FIGURE A.26: HSQC spectrum ($^1H = 700\ MHz\ and\ ^{13}C = 176\ MHz$, $DMSO - d_6$) of compound IIc.

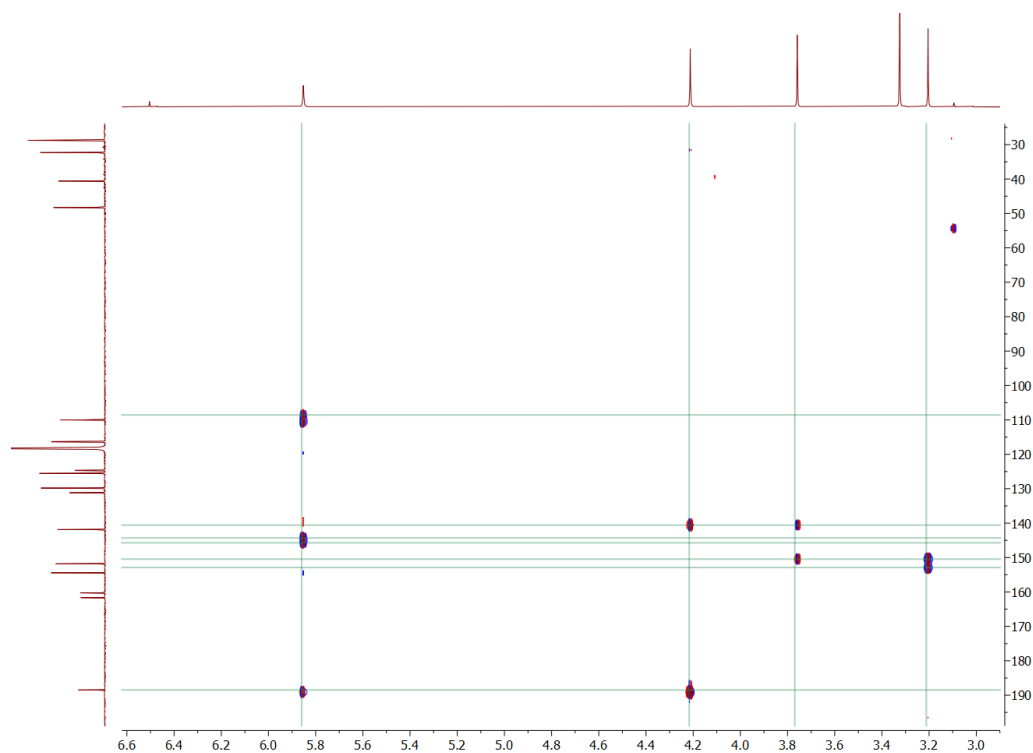FIGURE A.27: HSQC spectrum ($^1H = 700\ MHz\ and\ ^{13}C = 176\ MHz$, $DMSO - d_6$) of compound IId.

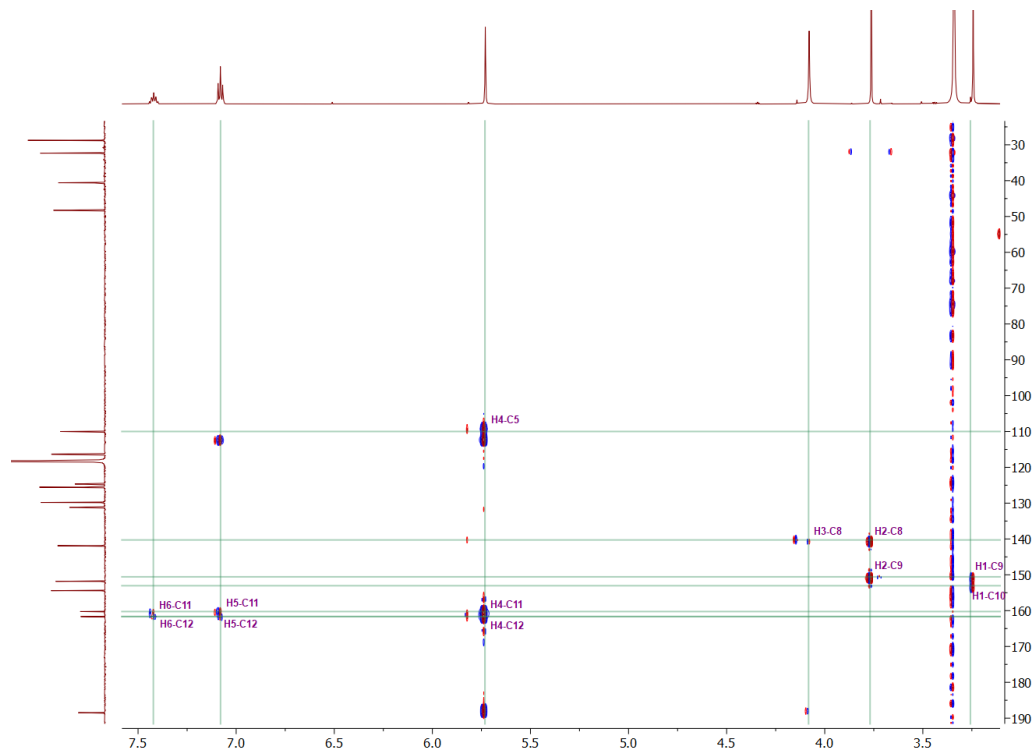FIGURE A.28: HSQC spectrum ($^1H = 700\ MHz\ and\ ^{13}C = 176\ MHz$, $DMSO - d_6$) of compound IIe.

Bibliography

(1) WHO Mortality and global health estimates, www.who.int, 2016.

(2) Observatory, T. G. C. Ecuador Fact Sheets, World Health Organization, 2020.

(3) Europe, A. W. H. O. R. O. F., *WORLD CANCER REPORT : cancer research for cancer development.* IARC Publications: 2020.

(4) Observatory, T. G. C. All cancers, World Health Organization, 2020.

(5) Hato, S. V.; Khong, A.; de Vries, I. J. M.; Lesterhuis, W. J. *Clinical Cancer Research* **2014**, *20*, 2831–2837.

(6) Savin, K. A., *Writing Reaction Mechanisms in Organic Chemistry*; Academic Press: 2014.

(7) Dotz, K. H., *Metal carbenes in organic synthesis*; Springer: 2004, pp 3–4.

(8) Crabtree, R. H., *The Organometallic Chemistry of the Transition Metals*; John Wiley Sons, Inc.: 2014.

(9) Cantat, T.; Mézailles, N.; Auffrant, A.; Le Floch, P. *Dalton Transactions* **2008**, 1957.

(10) Huynh, H. V., *The Organometallic Chemistry of N-heterocyclic Carbenes*; John Wiley Sons Ltd: 2017.

(11) A Patil, S.; P Hoagland, A.; A Patil, S.; Bugarin, A. *Future Medicinal Chemistry* **2020**, *12*, 2239–2275.

(12) Sánchez, A. T. Síntesis, Caracterización y Evaluación Citotóxica de Complejos NHC de Ir(I) Derivados de 5,6-dinitro-1H-benzol[d]imidazol, Ph.D. Thesis, 2019, pp 18–22.

(13) Valdés, H.; Canseco-González, D.; Germán-Acacio, J. M.; Morales-Morales, D. *Journal of Organometallic Chemistry* **2018**, *867*, 51–54.

(14) Chen, S.; Graceffa, R.; Boezio, A. *Organic Letters* **2016**, *18*, 16–19.

(15) Rufino-Felipe, E.; Colorado-Peralta, R.; Reyes-Márquez, V.; Valdés, H.; Morales-Morales, D. *Anti-Cancer Agents in Medicinal Chemistry* **2020**, *20*, DOI: 10.2174/1871520620666200908103452.

(16) Hopkinson, M. N.; Richter, C.; Schedler, M.; Glorius, F. *Nature* **2014**, *510*, 485–496.

(17) Nelson, D. R.; Nolan, S. P. *Chemical Society Reviews* **2013**, *42*, 6723–6723.

(18) Dröge, T.; Glorius, F. *Angewandte Chemie International Edition* **2010**, *49*, 6940–6952.

(19) Diez-Gonzalez, S., *N-heterocyclic carbenes : from laboratory curiosities to efficient synthetic tools*; Royal Society of Chemistry: 2017.

(20) Martínez, A.; Krinsky, J. L.; Peñafiel, I.; Castillón, S.; Loponov, K.; Lapkin, A.; Godard, C.; Claver, C. *Catalysis Science Technology* **2015**, *5*, 310–319.

(21) Yuan, D.; Teng, Q.; Huynh, H. V. *Organometallics* **2014**, *33*, 1794–1800.

(22) Visbal, R.; Gimeno, M. C. *Chem. Soc. Rev.* **2014**, *43*, 3551–3574.

(23) Mercs, L.; Albrecht, M. *Chemical Society Reviews* **2010**, *39*, 1903.

(24) Ye, J.; Mao, L.; Xie, L.; Zhang, R.-J.; Liu, Y.; Peng, L.; Yang, J.; Li, Q.; Yuan, M. *Front. Pharmacol.* **2021**, *12*, DOI: `10.3389/fphar.2021.753676`.

(25) Medici, S.; Peana, M.; Crisponi, G.; Nurchi, V. M.; Lachowicz, J. I.; Remelli, M.; Zoroddu, M. A. *Coordination Chemistry Reviews* **2016**, *327-328*, 349–359.

(26) Johnson, N. A.; Southerland, M. R.; Youngs, W. J. *Molecules* **2017**, *22*, 1263.

(27) Hussaini, S. Y.; Haque, R. A.; Razali, M. R. *Journal of Organometallic Chemistry* **2019**, *882*, 96–111.

(28) Institute, N. C. What Is Cancer?, National Cancer Institute, 2021.

(29) Organization, W. H. Cancer, Who.int, 2019.

(30) Nakashima, L. *Healthcare Management Forum* **2017**, *31*, 26–28.

(31) Ghosh, S. *Bioorganic Chemistry* **2019**, *88*, 102925.

(32) Rosenberg, B *Cisplatin* **1980**, 9–20.

(33) Johnstone, T. C.; Suntharalingam, K.; Lippard, S. J. *Philosophical Transactions of the Royal Society A: Mathematical, Physical and Engineering Sciences* **2015**, *373*, 20140185.

(34) LALLIER, R *Cell Biology International Reports* **1980**, *4*, 697–700.

(35) Johnstone, T. C.; Suntharalingam, K.; Lippard, S. J. *Chemical Reviews* **2016**, *116*, 3436–3486.

(36) J. Anthony, E.; M. Bolitho, E.; E. Bridgewater, H.; L. Carter, O. W.; M. Donnelly, J.; Imberti, C.; C. Lant, E.; Lermyte, F.; J. Needham, R.; Palau, M.; J. Sadler, P.; Shi, H.; Wang, F.-X.; Zhang, W.-Y.; Zhang, Z. *Chemical Science* **2020**, *11*, 12888–12917.

(37)   Yan, Y. K.; Melchart, M.; Habtemariam, A.; Sadler, P. J. *Chemical Communications* **2005**, 4764.

(38)   Dougan, S. J.; Sadler, P. J. *CHIMIA International Journal for Chemistry* **2007**, *61*, 704–715.

(39)   Haque, R. A.; Iqbal, M.; Asekunowo, P. O.; Majid, A.; Khadeer, M. B.; Umar, M.; Al-Rawi, S. S.; Fouad *Medicinal Chemistry Research* **2013**, *22*, 4663–4676.

(40)   Dolbier, W. R., *Guide to fluorine NMR for organic chemists*; John Wiley amp; Sons, Inc.: 2016.

(41)   Hameury, S.; de Frémont, P.; R. Breuil, P.-A.; Olivier-Bourbigou, H.; Braunstein, P. *Dalton Trans.* **2014**, *43*, 4700–4710.